Journal of Wind Engineering & Industrial Aerodynamics 232 (2023) 105279

Contents lists available at ScienceDirect

Journal of Wind Engineering & Industrial Aerodynamics

journal homepage: www.elsevier.com/locate/jweia

Improved estimation of time-varying mean displacement and parametric study of biaxial effect on inelastic responses of high-rise buildings to wind

Jinghui Huang, Xinzhong Chen *

National Wind Institute, Department of Civil, Environmental and Construction Engineering, Texas Tech University, Lubbock, TX, 79409-1023, USA

ARTICLE INFO

Keywords:
High-rise building
Bouc-Wen hysteresis model
Biaxial effect
Inelastic response
Peak ductility demand

ABSTRACT

Three reduced-order building models with different biaxial hysteretic generalized restoring force and displacement relations were developed using static modal pushover analysis of a nonlinear finite element model of a 60-story steel building. It was illustrated that the reduced-order models can give accurate estimations of fluctuating responses but overestimate the time-varying mean alongwind displacement. The nonphysical displacement drift of the Bouc-Wen hysteresis model is responsible for this overestimation. An improved estimation of time-varying mean alongwind displacement was presented. A comprehensive parametric study concerning the influence of biaxial interaction on inelastic responses was also performed. The biaxial interaction leads to faster growth of time-varying mean displacement but does not affect its steady-state value. It results in increase in the low-frequency component but decrease in the resonant component of alongwind displacement. It leads to more reduction in alongwind acceleration. The crosswind response, which is greater than the alongwind response, is not affected, or only slightly reduced when both alongwind and crosswind responses are close to each other in magnitude. The peak ductility demand of a combined alongwind and crosswind response is less affected by the biaxial interaction. The new insights of this study can have wide applications to other buildings and wind directions.

1. Introduction

Current design of tall buildings to wind has been based on linear elastic performance of structures. Recent development of performance-based wind design of tall buildings has pushed the envelope of linear elastic framework, permitting limited level of inelasticity, thus asking for improved understanding of wind-induced inelastic structural performance. The adoption of inelastic design framework has potential to achieve safer and more economic design solutions (ASCE/SEI, 2019).

The inelastic performance of wind-excited tall buildings has been studied in literature (Ohkuma et al., 1997; Tsujita et al., 1997; Tamura et al., 2001; Hong, 2004; Hart and Jain, 2011; Gani and Légeron, 2012; Griffis et al., 2013; Beck et al., 2014; Judd and Charney, 2015, 2016; Mooneghi et al., 2015; Judd, 2018; Mohammadi et al., 2019; Ghaffary and Moustafa, 2021; Ouyang and Spence, 2021). The building models used in analysis range from a single-degree-of-freedom (SDOF) model to a two-dimensional (2D) and three-dimensional (3D) multiple-degree-of-freedom (MDOF) nonlinear finite element (FE) model with distributed plasticity (NIST, 2010). Huang and Chen (2022) conducted a comprehensive analysis of inelastic response of tall buildings under simultaneous actions of both alongwind and crosswind loads based on a 3D nonlinear FE model of a 60-story building. The second-order P-Delta effect on both elastic and inelastic responses was also examined. The nonlinear FE building model with distributed plasticity can provide detailed information of inelastic response characteristics but is computationally very expensive.

On the other hand, a reduced-order building model in terms of fundamental building modal responses can be developed with improved computational efficiency. Feng and Chen (2017, 2018) presented a comprehensive study on both alongwind and crosswind responses by considering the fundamental mode with bilinear restoring force character through time history analysis and statistical linearization approach. Huang and Chen (2023) carried out inelastic building response analysis using a reduced-order building model, in which the building response was represented by fundamental modal displacements, and the hysteretic relations between the generalized restoring forces and displacements were determined by static modal push-over analysis (MPA) using a nonlinear FE building model. These relations

* Corresponding author.
E-mail addresses: jinghui.huang@ttu.edu (J. Huang), xinzhong.chen@ttu.edu (X. Chen).

https://doi.org/10.1016/j.jweia.2022.105279
Received 27 July 2022; Received in revised form 28 November 2022; Accepted 12 December 2022
0167-6105/© 2022 Elsevier Ltd. All rights reserved.

were then represented by a biaxial hysteretic force model (Wang and Wen, 2000) in which the restoring forces in two translational directions are coupled and have hysteretic relations with building displacements in both translational directions. Due to the coupling of restoring forces, the alongwind and crosswind building responses need to be evaluated simultaneously using the coupled equations of motion. The coupling effect is referred to as biaxial interaction of alongwind and crosswind responses. On the other hand, when the biaxial interaction is ignored, the equations of motion become uncoupled. Subsequently, the alongwind and crosswind inelastic responses can be computed separately like the linear response analysis. The accuracy of the reduced-order building model in predicting fluctuating responses has been verified, while the time-varying mean alongwind displacement is overestimated as compared to the prediction using nonlinear FE model (Huang and Chen, 2023).

In the reduced-order building model, the relations of the generalized restoring forces and displacements are presented by Bouc-Wen hysteretic model (Wang and Wen, 2000). The Bouc-Wen model belongs to the family of endochronic models, which introduces a differential equation for an extra variable (hysteretic displacement) to describe the hysteretic relation. It is known that this type of model exhibits displacement drift, force relaxation and nonclosure of hysteretic loops under intermediate unloading-reloading path (Thyagarajan 1989; Wong et al., 1994; Charalampakis and Koumousis, 2009). The Bouc-Wen model does not differentiate between virgin loading and reloading thus leads to reduced reloading stiffness as compared to the unloading one (Charalampakis and Koumousis, 2009). Wong et al. (1994) suggests use of a hysteresis model with a sharp transition from linear elastic to plastic to reduce the nonphysical behavior. However, it will result in similar behavior of bilinear model and will reduce the accuracy when the equivalent linearization approach is used. Charalampakis and Koumousis (2009) proposed a modified uniaxial hysteretic model by introducing a stiffening factor which enables the distinction between virgin loading and reloading. The overestimation of the time-varying mean alongwind displacement in the reduced-order model (Huang and Chen, 2023) may be related to the nonphysical behavior of the Bouc-Wen model.

This study will examine the sensitivity of the time-varying mean and fluctuating inelastic response of a 60-story steel building to hysteretic restoring force model parameters, which is important for the development of reduced-order building model to achieve computational accuracy and efficiency. The cause for the overestimation of time-varying mean alongwind displacement will be investigated from the perspective of nonphysical behavior of Bouc-Wen hysteresis model. A modified uniaxial hysteretic model and modification of biaxial hysteresis model will be examined for a better estimation of time-varying mean alongwind displacement. This study will also present a comprehensive parametric study on the influence of biaxial interaction on time-varying mean displacement and standard deviations (STDs) of fluctuating responses in terms of wide ranges of yielding levels of alongwind and crosswind responses, their correlation, and others. This parametric study leads to fundamental understanding of the interaction of inelastic alongwind and crosswind responses of tall buildings to wind.

2. Inelastic response analysis using a reduced-order building model

A reduced-order two degree-of-freedom (2DOFs) nonlinear building model can be developed through static MPA procedure using a nonlinear FE building model (Huang and Chen, 2023). The static loads in both translational x and y directions that follow heightwise distributions of fundamental modal inertial loads are applied to the FE building model. The fundamental mode shapes are evaluated from the linear building model. The magnitudes of the loads are monotonically increased, and the corresponding building displacements are calculated. The generalized restoring forces F_{sx} and F_{sy} are calculated from the distributed forces and modal shapes. The analysis is repeated for different combinations of F_{sx} and F_{sy}, which leads to hysteretic relations of the generalized hysteretic restoring forces and generalized displacements (building top displacements) in both directions. When load is only applied in one direction, the uniaxial hysteretic relation of the restoring force and displacement is established.

By assuming that the heightwise distributions of inelastic building response follow the distributions of fundamental mode shapes of the linear building model, the coupled equations of generalized modal displacements are described as:

$$M_x\ddot{q}_x + 2M_x\zeta_x\omega_x\dot{q}_x + F_{sx}\left(q_x, \dot{q}_x, q_y, \dot{q}_y\right) = Q_x \tag{1a}$$

$$M_y\ddot{q}_y + 2M_y\zeta_y\omega_y\dot{q}_y + F_{sy}\left(q_x, \dot{q}_x, q_y, \dot{q}_y\right) = Q_y \tag{1b}$$

where $q_x(t)$ and $q_y(t)$ are generalized displacements in terms of building top displacements; M_x, ω_x, ζ_x, $Q_x(t)$ and M_y, ω_y, ζ_y, $Q_y(t)$ are generalized mass, modal frequency, damping ratio, and generalized wind load in two directions of the corresponding linear system; F_{sx} and F_{sy} are generalized restoring forces. When building response is within linear elastic range, $F_{sx}(q_x, \dot{q}_x, q_y, \dot{q}_y) = K_x q_x = M_x\omega_x^2 q_x$, and $F_{sy}(q_x, \dot{q}_x, q_y, \dot{q}_y) = K_y q_y = M_y\omega_y^2 q_y$, thus the equations of linear modal responses are uncoupled. When building behaves beyond linear elastic range, the generalized restoring forces have hysteretic relations with displacements in both translational directions. As a result, the equations of motion become coupled.

The generalized restoring forces F_{sx} and F_{sy} are then fitted into the following biaxial hysteretic model (Wang and Wen, 2000):

$$F_{sx} = \alpha_x K_x q_x + (1-\alpha_x)K_x z_x \tag{2a}$$

$$F_{sy} = \alpha_y K_y q_y + \left(1-\alpha_y\right)K_y z_y \tag{2b}$$

$$\dot{z}_x = A_x\dot{q}_x - z_x I \tag{3a}$$

$$\dot{z}_y = A_y\dot{q}_y - z_y I \tag{3b}$$

$$I = \left\{|\dot{q}_x||z_x|\left[\beta_0 + \gamma_0 \mathrm{sgn}(\dot{q}_x z_x)\right] \Big/ \Delta_x^2 + |\dot{q}_y||z_y|\left[\beta_0 + \gamma_0 \mathrm{sgn}\left(\dot{q}_y z_y\right)\right] \Big/ \Delta_y^2\right\} \times \left[\left(z_x/\Delta_x\right)^2 + \left(z_y/\Delta_y\right)^2\right]^{\frac{n-2}{2}} \tag{3c}$$

where α_x and α_y are second (post-yielding) stiffness ratios; z_x and z_y are hysteretic displacements; sgn $(\cdot)$ is sign function; $A_x = A_y = 1$ in general; Δ_x and Δ_y are generalized yield displacements under uniaxial loads in x and y directions, respectively. The shape parameter n determines the smoothness of transition from pre-yielding to post-yielding region; $\beta_0 + \gamma_0 = 1$, and often $\beta_0 = \gamma_0 = 0.5$.

To better understand the yield displacement boundary under biaxial loads, the displacement q_0 and hysteretic displacement z_0 for a displacement path along Θ-axis are considered, defined by a line passing the origin in the q_x/Δ_x and q_y/Δ_y plane with a counterclockwise rotation angle θ from q_x/Δ_x (Lee and Hong, 2010). As $q_x/\Delta_x = q_0\cos\theta$, $q_y/\Delta_y = q_0\sin\theta$, $z_x/\Delta_x = z_0\cos\theta$, $z_y/\Delta_y = z_0\sin\theta$, $A_x = A_y = A_0$, Eq. (3)

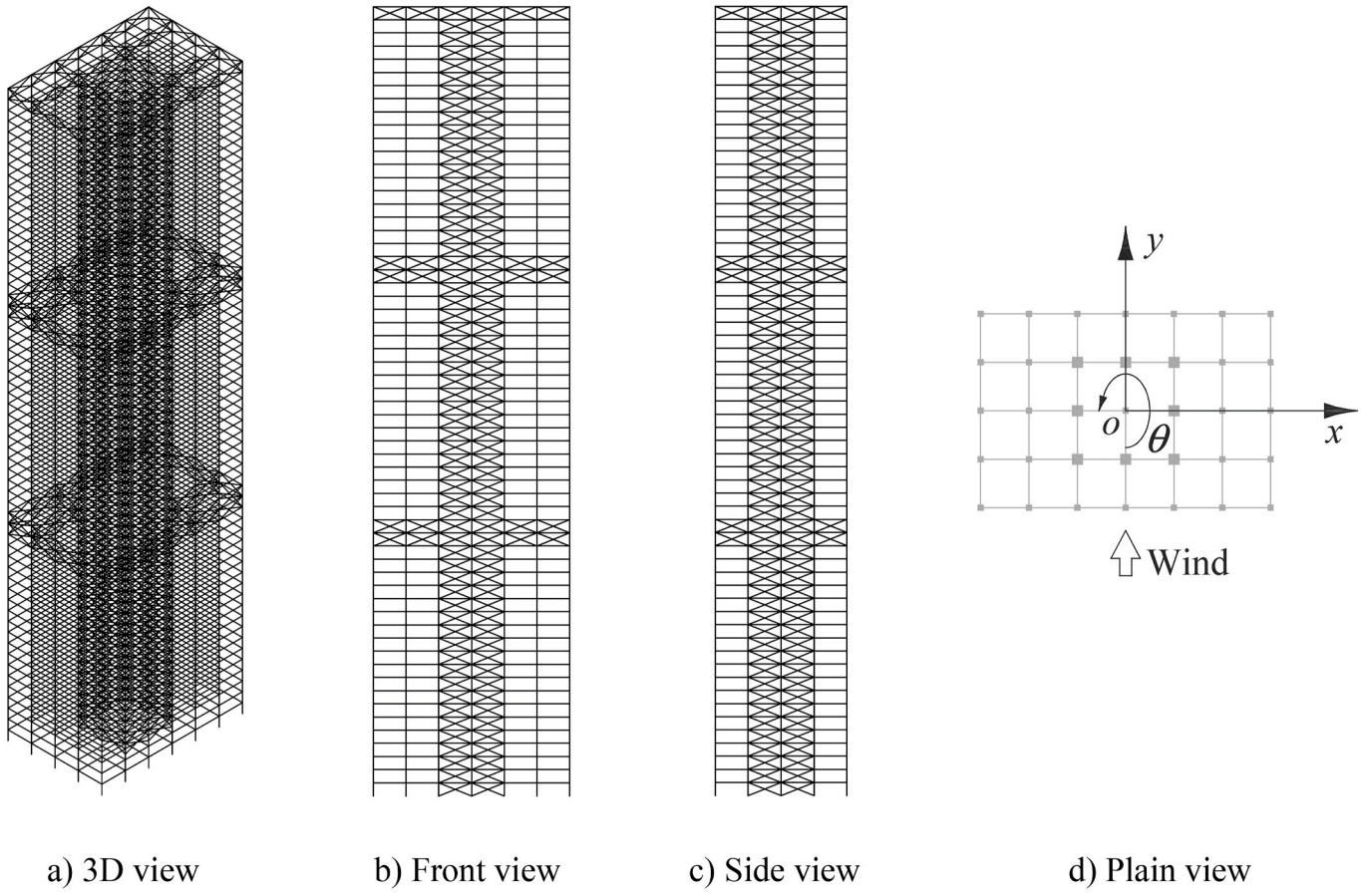

Fig. 1. FE model of the 60-story steel building frame.

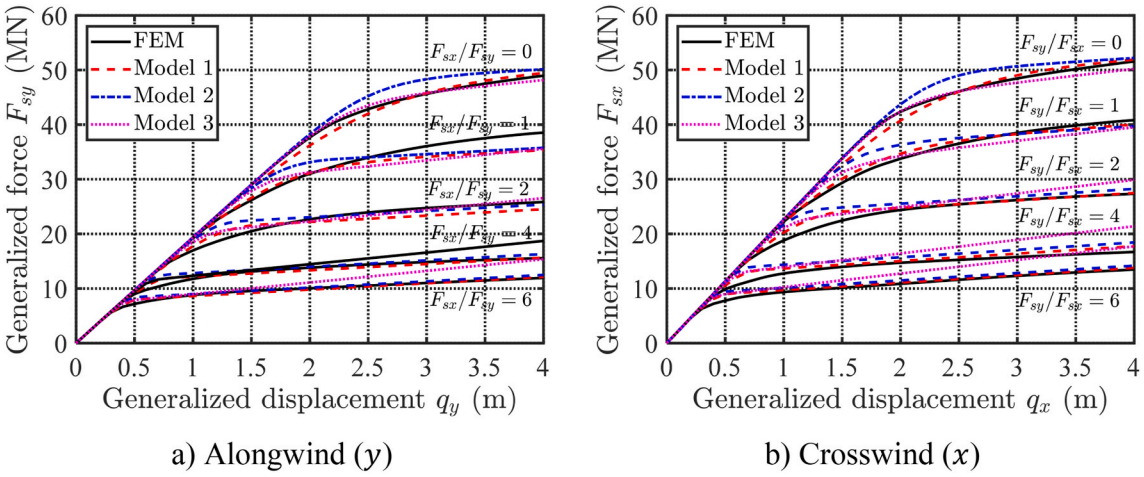

Fig. 2. Generalized restoring force and deformation relations.

becomes:

$$\dot{z}_0 = \dot{q}_0 - z_0 I_0 \tag{4a}$$

$$I_0 = |\dot{q}_0||z_0|^{n-1}[\beta_0 + \gamma_0 \mathrm{sgn}(\dot{q}_0 z_0)] \tag{4b}$$

The normalized yield displacement along the Θ-axis, $\Delta_0(\theta) = |z_{0u}(\theta)| = 1$, is obtained by setting $\dot{z}_0 = 0$, and same sign for $\dot{q}_0$ and z_0 (Lee and Hong, 2010). The yielding displacements in both directions are $\Delta_x(\theta) = \Delta_0(\theta)\Delta_x \cos\theta = \Delta_x \cos\theta$ and $\Delta_y(\theta) = \Delta_0(\theta)\Delta_y \sin\theta = \Delta_y \sin\theta$. Obviously, the yield boundary in the $\Delta_x(\theta)/\Delta_x$ and $\Delta_y(\theta)/\Delta_y$ plane form a circle. The biaxial model is isotropic, indicating equal interaction of two directions.

The ductility factors of both displacements and their combined response are defined as:

$$\mu_x(t) = |q_x(t)| \,/\, \Delta_x, \mu_y(t) = |q_y(t)| \,/\, \Delta_y \mu(t) = \left[|q_x(t)/\Delta_x|^2 + |q_y(t)/\Delta_y|^2\right]^{1/2} \tag{5}$$

The equations of building motion are represented in state-space equations and are then solved by using step-by-step integration

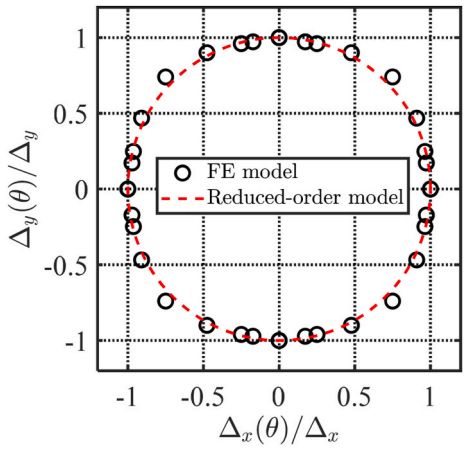

Fig. 3. Yield displacement boundary of the FE and hysteresis models.

Table 1
Parameters of three hysteretic force models.

	K_y (kN/m)	K_x (kN/m)	Δ_y (m)	Δ_x (m)	n	α_y	α_x
Model 1	19366	22622	2.5	2.2	4	0.06	0.06
Model 2	19366	22622	2.5	2.2	9	0.06	0.06
Model 3	19366	22622	2.3	2.0	9	0.11	0.11

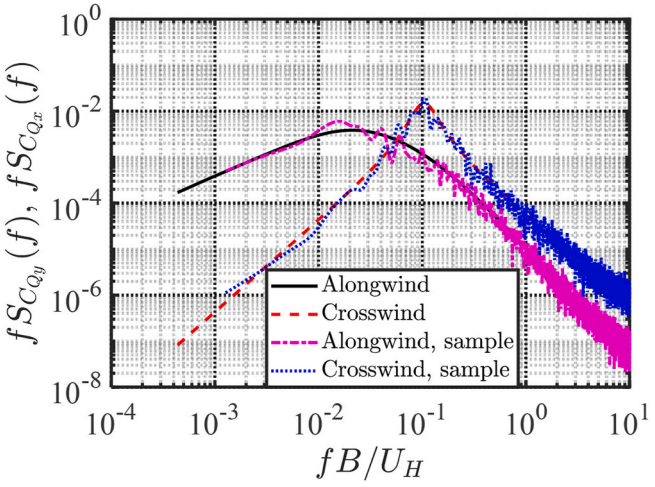

Fig. 4. Power spectra of generalized force coefficients.

method, such as fourth order Runge-Kutta method. The generalized dynamic wind load time history samples are simulated from loading power spectra using spectral representation method (Shinozuka and Jan 1972; Chen and Kareem, 2005a).

3. Building example

A 60-story high-rise steel structure with 182.88 m height, 45.72 m width, and 30.48 m depth is considered (Fig. 1). The building has an outrigger system at three elevations, i.e., 20th and 21st, 40th and 41st, and 60th floors, and a core bracing system to resist the lateral load. A 3D nonlinear FE model is constructed in the OpenSees environment (McKenna et al., 2010). The building frame is consisted of 2,100 columns, 3,480 beams, and 2,560 diagonal bracings, including a total of 16 types of member sections. All members are modeled in fiber-type nonlinear element models (NIST, 2010) and each element has five fiber sections. More than 300 fibers over each column and bracing cross-sectional area, and more than 150 fibers over each beam cross-sectional area are used. The typical column length is 3,048 mm and the typical beam length is 7,620 mm. The mass of the structure was concentrated at the nodes. The slabs were considered as rigid diaphragms. The nonlinearity of the steel material is described by a bilinear hysteretic model with a yield stress of 345 MPa and a post-yielding stiffness ratio of 0.01. The two fundamental frequencies in two translational directions, i.e., x and y directions, are $f_x = 0.173$ Hz and $f_y = 0.164$ Hz. The modal damping ratios are assumed to be $\zeta_x = \zeta_y = 1\%$. The fundamental mode shapes are close to linear variations. More detailed information about the FE model can be found in Park and Yeo (2018) and Huang and Chen (2022). The torsional wind load and response are quite low thus are not considered in this study. The torsional response can be important for buildings with non-regular configurations and lower structural stiffness for torsion. The mean wind speed is along y direction, thus $B = 45.72$ m and $D = 30.48$ m.

Fig. 2 shows the generalized restoring force-displacement relations for a given ratio F_{sy}/F_{sx}, where $F_{sy}/F_{sx} = 0$ and $F_{sx}/F_{sy} = 0$ correspond to the cases of uniaxial loads in x and y directions, respectively. For a given ratio F_{sy}/F_{sx}, the generalized restoring force-displacement relation in each direction is fitted into a uniaxial hysteretic model, from which the generalized yield displacements are determined, denoted as $\Delta_x(\theta)$ and $\Delta_y(\theta)$, respectively, for x and y directions. The corresponding direction is defined as $\theta = \arctan\{[\Delta_y(\theta)/\Delta_y]/[\Delta_x(\theta)/\Delta_x]\}$, which is also $\theta = \arctan\{[F_{sy}/K_y\Delta_y(\theta)]/[F_{sx}/K_x\Delta_x(\theta)]\}$ in the linear elastic range. With this information, the yield displacement boundary is constructed as shown in Fig. 3, which is close to a circle and is consistent to that from the biaxial hysteretic model. The yield displacement in one direction reduces due to the influence of load in another direction.

Three different biaxial models are fitted, and the model parameters

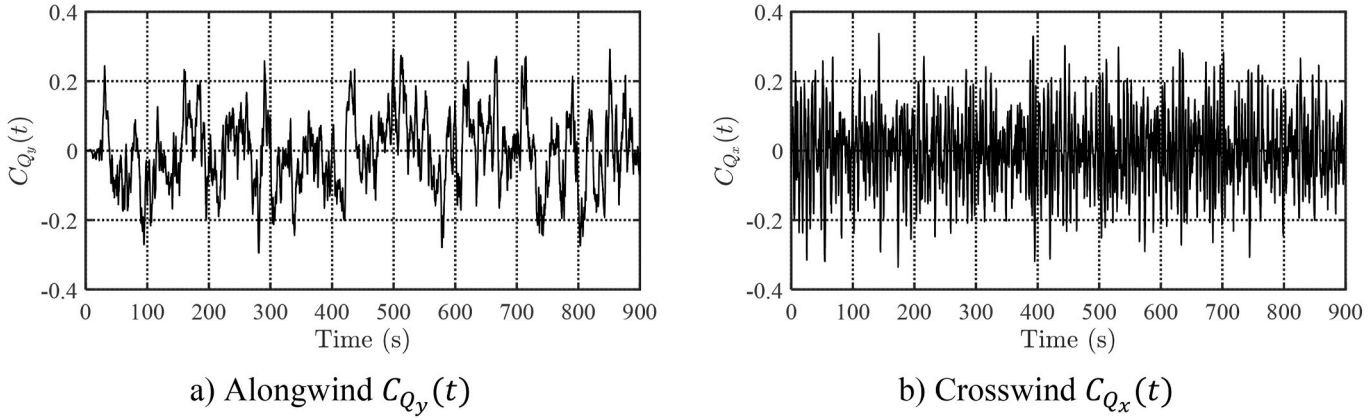

Fig. 5. Time history samples of the generalized force coefficients ($U_H = 80$ m/s).

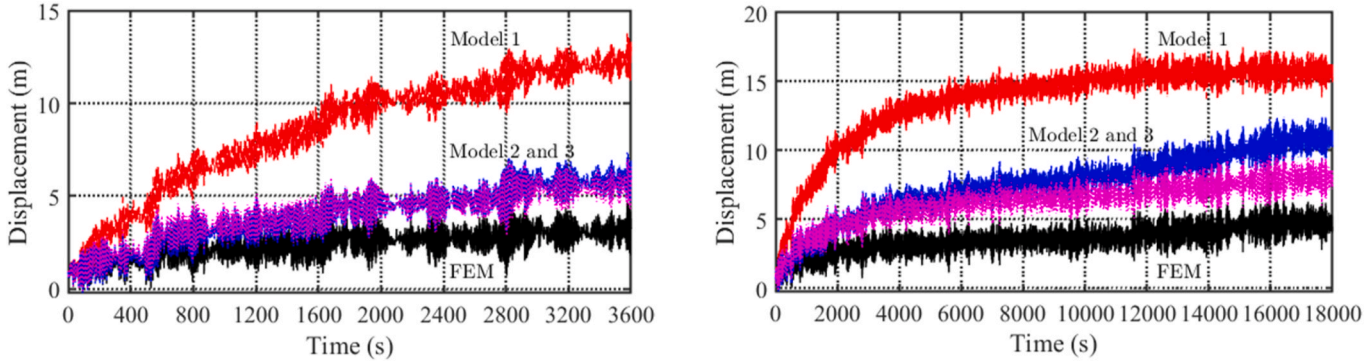

a) Time history sample, t=0-3,600 s, $U_H = 80$ m/s

b) Time history sample, t=0-18,000 s, $U_H = 80$ m/s

Fig. 6. Comparison of alongwind building top displacement estimated from different models (uniaxial loads).

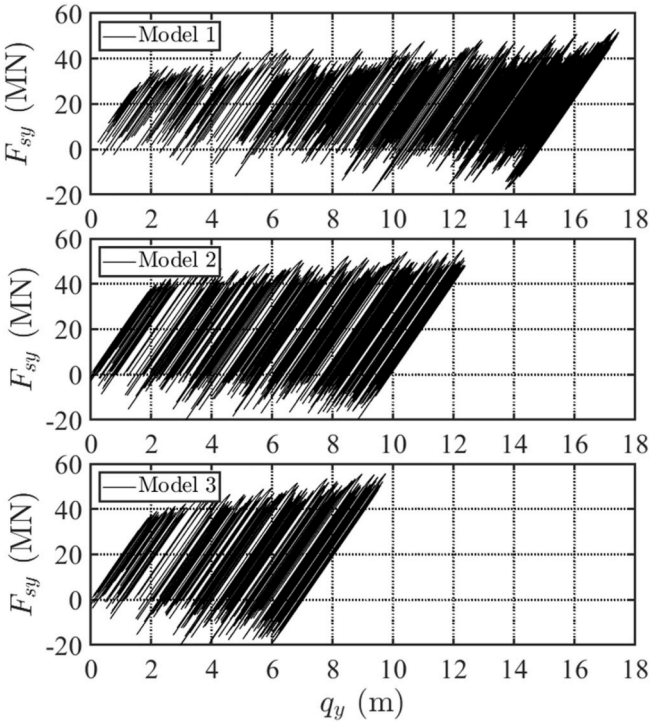

Fig. 7. Relation of generalized alongwind hysteretic force and displacement (uniaxial loads, $U_H = 80$ m/s, t = 0–18,000 s).

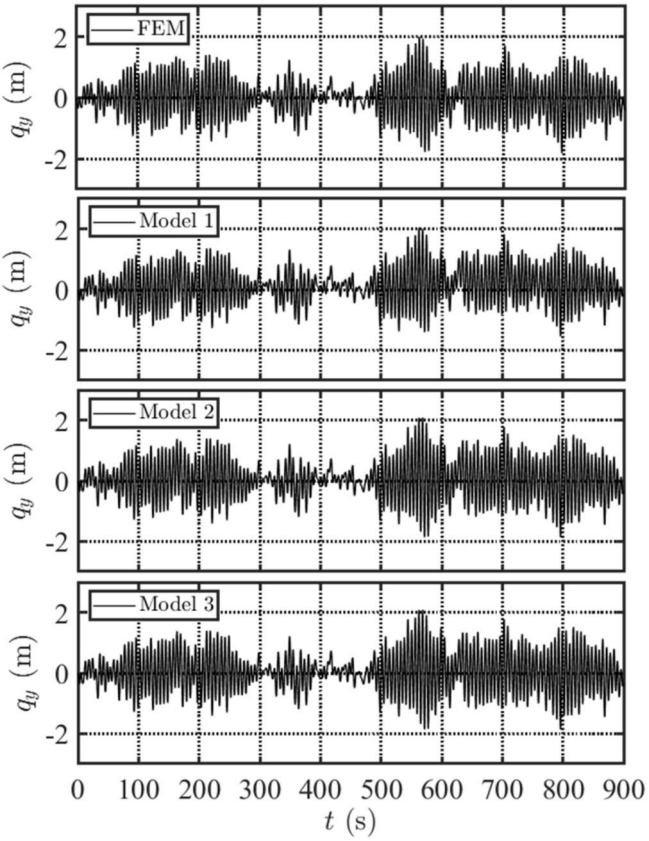

Fig. 8. Comparison of alongwind building top displacement without mean wind load (uniaxial loads, $U_H = 80$ m/s).

are listed in Table 1. All these models have same generalized linear pre-yield stiffness. Models 1 and 2 have same yield displacements and post-yield stiffness ratios, but Model 2 has a larger value of model parameter n, i.e., sharp transition from pre-yield to post-yield regions. Model 3 has same parameter n as Model 2, but larger post-yield stiffness and slightly lower yield displacements. Model 1 was used in Huang and Chen (2023). In these biaxial hysteretic models, the relationships of restoring forces and displacements in two directions under a given ratio F_{sy}/F_{sx} are completely defined by the uniaxial force models at $F_{sy}/F_{sx} = 0$ and $F_{sx}/F_{sy} = 0$ and the ratio F_{sy}/F_{sx}. These biaxial hysteretic models are approximate representations of actual behavior of the real building. Some differences between the fitted models and FEM results shown in Fig. 2 are expected. The accuracy and sensitivity of building response estimated from these models will be investigated as compared to that from the FE model.

4. Wind loading model

The alongwind static wind force at i-th story is determined as:

$$\overline{P}_i = 0.5\rho U_H^2 \overline{C}_D B H_0 \left(\frac{z_i}{H}\right)^{2\alpha_s} \tag{6}$$

where $\rho = 1.22$ kg/m^3 is the air density,; U_H is the mean wind speed at the building top averaged in 10 min; B is the building width; H_0 is the story height; H is the building height above the ground; z_i is the height of i-th floor; $\overline{C}_D$ is the constant drag force coefficient along the building height and is related to the static coefficient of base bending moment $\overline{C}_M$

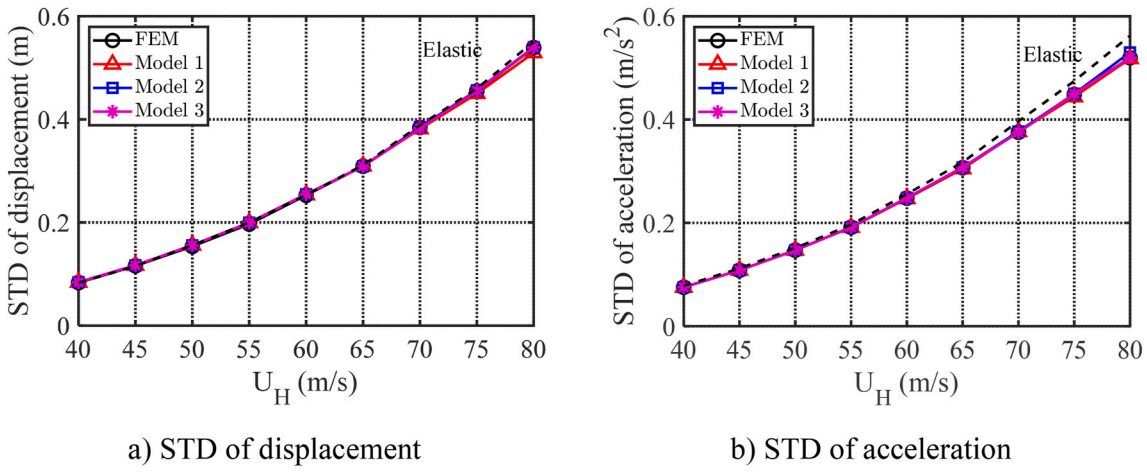

Fig. 9. STDs of alongwind response under different wind speeds (uniaxial loads).

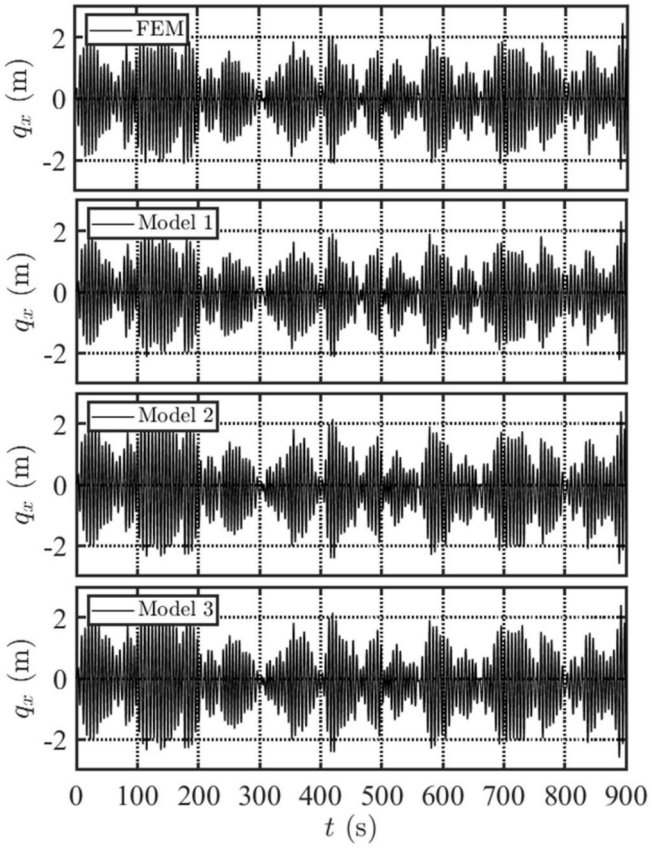

Fig. 10. Comparison of crosswind building top displacement (uniaxial loads, $U_H = 80$ m/s).

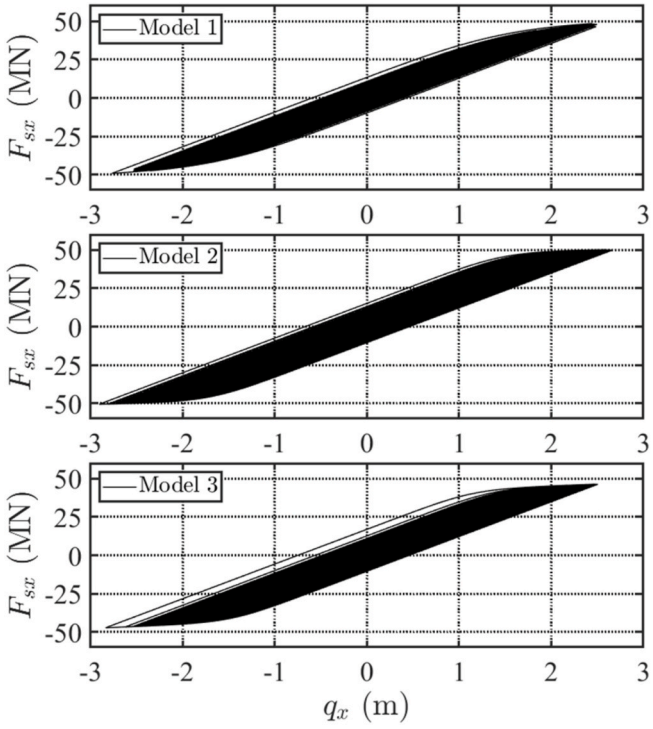

Fig. 11. Relation of generalized crosswind hysteretic force and displacement (uniaxial loads, $U_H = 80$ m/s, $t = 0$–18,000 s).

as $\overline{C}_D = 2\overline{C}_M(\alpha_s + 1)$ according to the static wind loading model shown in Eq. (6); $\alpha_s = 0.2$ is the power law exponent of the wind speed profile for the suburban terrain. The wind loading information in term of base bending moment coefficient is often directly measured in wind tunnel using high-frequency force balance technique.

The fluctuating components of alongwind story forces are modeled in terms of power spectra density (PSD) model, which is established based on wind tunnel data. The cross power spectral density (CPSD) function of the i-th and j-th story forces is given as (Chen and Kareem, 2005a):

$$S_{P_iP_j}(f) = S_{P_0}(f)\left(\frac{z_i}{H}\right)^{\alpha_s}\left(\frac{z_j}{H}\right)^{\alpha_s}\exp\left(-\frac{k_z f H}{U_H}\frac{|z_i - z_j|}{H}\right) \tag{7}$$

$$S_{P_0}(f) = \left(\frac{1}{2}\rho U_H^2 B H_0\right)^2 S_{C_M}(f) \Big/ |J_z(f)|^2 \tag{8}$$

$$|J_y(f)|^2 = \left(\frac{H_0}{H}\right)^2 \sum_{i=1}^{N}\sum_{j=1}^{N}\left(\frac{z_i}{H}\right)^{\alpha_s+1}\left(\frac{z_j}{H}\right)^{\alpha_s+1}\exp\left(-\frac{k_z f H}{U_H}\frac{|z_i - z_j|}{H}\right) \tag{9}$$

where $S_{C_M}(f)$ is the PSD of the base bending moment coefficient $C_M(t)$; $k_z = 7$ is the decay factor for the alongwind load; and $N = 60$ is the number of stories. Same CPSD model is also used for crosswind story forces, but different spectrum $S_{C_M}(f)$ and decay factor $k_z = 5$ are adopted. The alongwind and crosswind loads are assumed to be mutually

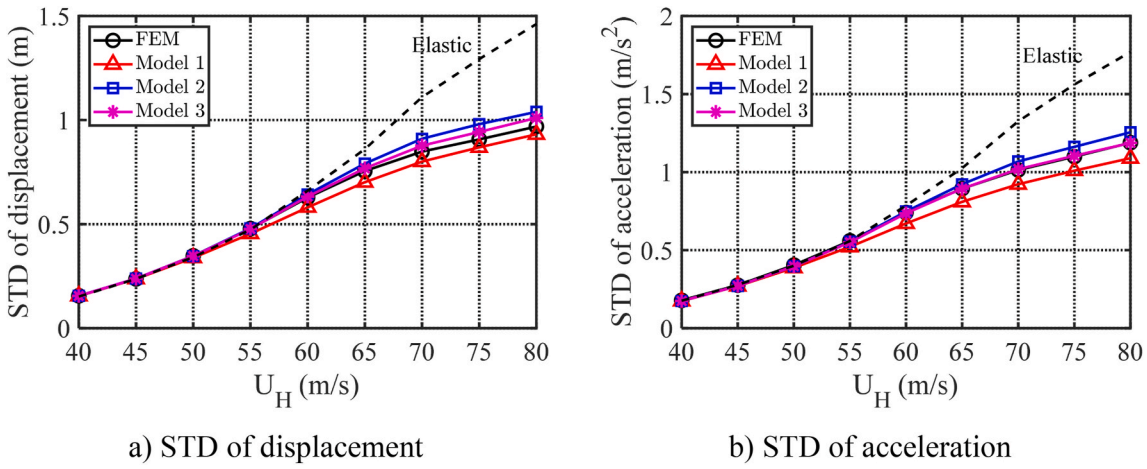

Fig. 12. STDs of crosswind response under different wind speeds (uniaxial loads).

Table 2
Response STDs calculated from FE model and three hysteretic models (U_H = 80 m/s, Unit: Disp., m; Acce., m/s^2).

	Linear Elastic				Uniaxial Model				Biaxial Model			
	Alongwind		Crosswind		Alongwind		Crosswind		Alongwind		Crosswind	
	Disp.	Acce.	Disp.	Acce.	Disp.	Acce.	Disp.	Acce.	Disp.	Acce.	Disp.	Acce.
FE model	0.55	0.56	1.46	1.77	0.54	0.52	0.97	1.19	0.46	0.42	0.94	1.15
Model 1	0.55	0.56	1.46	1.77	0.53	0.52	0.93	1.09	0.45	0.41	0.91	1.06
Model 2	0.55	0.56	1.46	1.77	0.54	0.53	1.04	1.25	0.46	0.45	1	1.21
Model 3	0.55	0.56	1.46	1.77	0.54	0.52	1.01	1.19	0.47	0.43	0.96	1.15

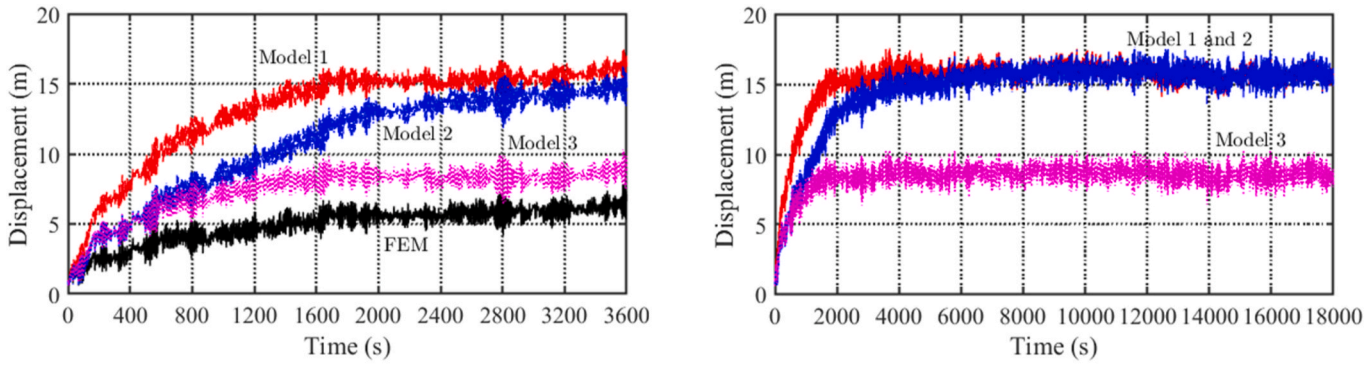

Fig. 13. Comparison of alongwind building top displacement under biaxial loads.

independent according to extensive wind tunnel data of tall building models with various rectangular cross-sections (e.g., AIJ, 2004). In this study, the motion-induced wind load and vortex-induced vibration in crosswind direction, referred to aeroelastic effects (e.g., Chen, 2013, 2014a and 2014b), are not considered. At higher wind speeds the hysteretic restoring force caused by yielding of building members introduces significant additional damping, thus the aeroelastic effects become less important for inelastic response as compared to linear elastic response (Feng and Chen, 2017).

The PSDs of alongwind and crosswind $C_M(t)$ are given according to Architectural Institute of Japan (AIJ) recommendations (AIJ, 2004; Ding and Chen, 2015). The standard deviation (STD) of alongwind $C_M(t)$ is σ_{C_M} = 0.110. For crosswind, σ_{C_M} = 0.118; the bandwidth parameter of the spectrum takes β_1 = 0.28; parameter κ_1 = 0.85; and the Strouhal number S_t = 0.104. The PSDs of the generalized forces $Q_x(t)$ and $Q_y(t)$ are then calculated from the CPSD model of story forces and are used for generation of their time history samples using spectral representation method.

Fig. 4 shows the power spectra of the generalized force coefficients in alongwind and crosswind directions, i.e., $C_{Q_y}(t) = Q_y(t)/(0.5\rho U_H^2 BH)$ and $C_{Q_x}(t) = Q_x(t)/(0.5\rho U_H^2 BH)$, which are very close to the PSDs of the base bending moment coefficients. The STDs of $C_{Q_y}(t)$ and $C_{Q_x}(t)$ are 0.109 and 0.116. The power spectrum of alongwind loading has higher low-frequency energy, while the power spectrum of crosswind loading exhibits a peak at the lock-in reduced frequency, $fB/U_H = S_t$ = 0.104. Fig. 5 shows the time history samples of $C_{Q_y}(t)$ and $C_{Q_x}(t)$ at U_H = 80 m/s. The PSDs calculated from loading samples are also shown in Fig. 4, which meets the target PSDs.

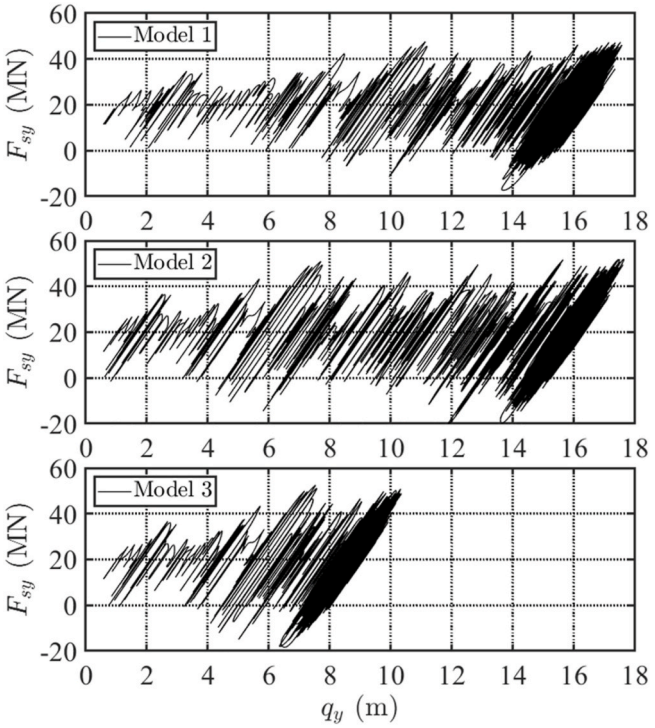

Fig. 14. Alongwind hysteretic force and displacement relation (biaxial loads, $U_H = 80$ m/s, $t = 0$–18,000 s).

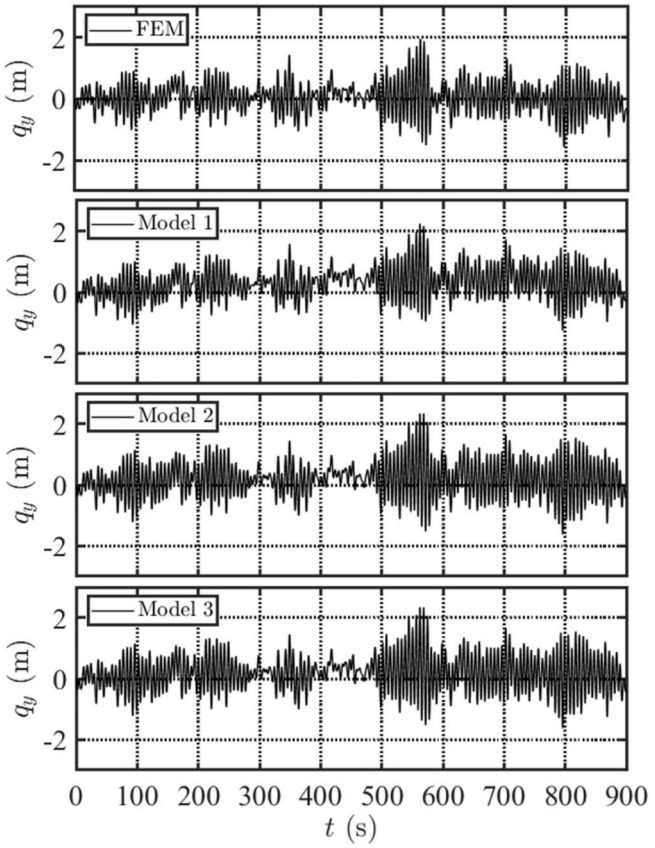

Fig. 15. Comparison of alongwind building top displacement without the mean wind load (biaxial loads, $U_H = 80$ m/s).

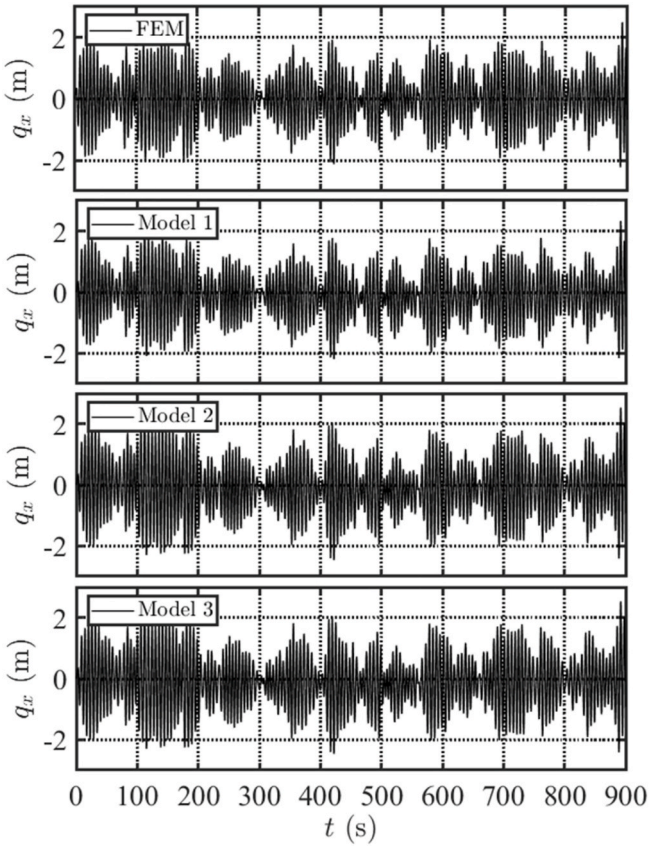

Fig. 16. Comparison of crosswind building top displacement (biaxial loads, $U_H = 80$ m/s).

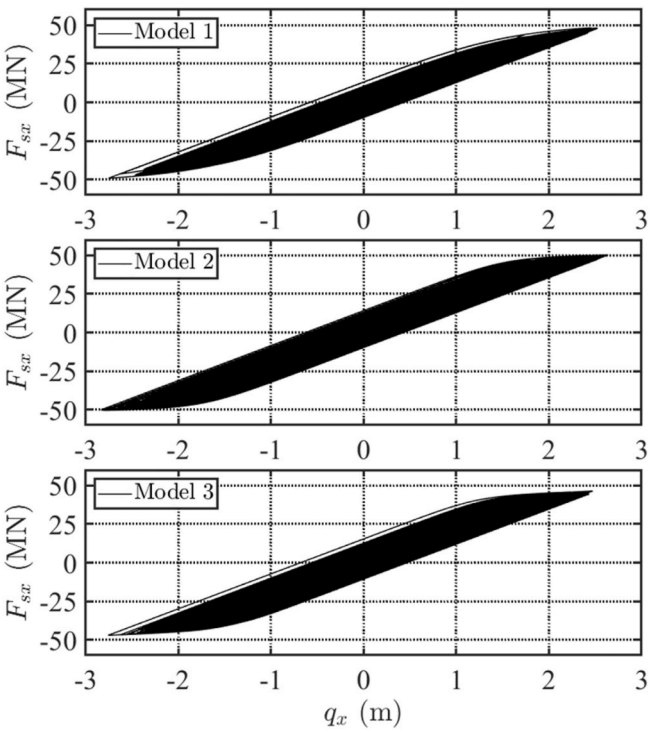

Fig. 17. Crosswind hysteretic force and displacement relation (biaxial loads, $U_H = 80$ m/s, $t = 0$–18,000 s).

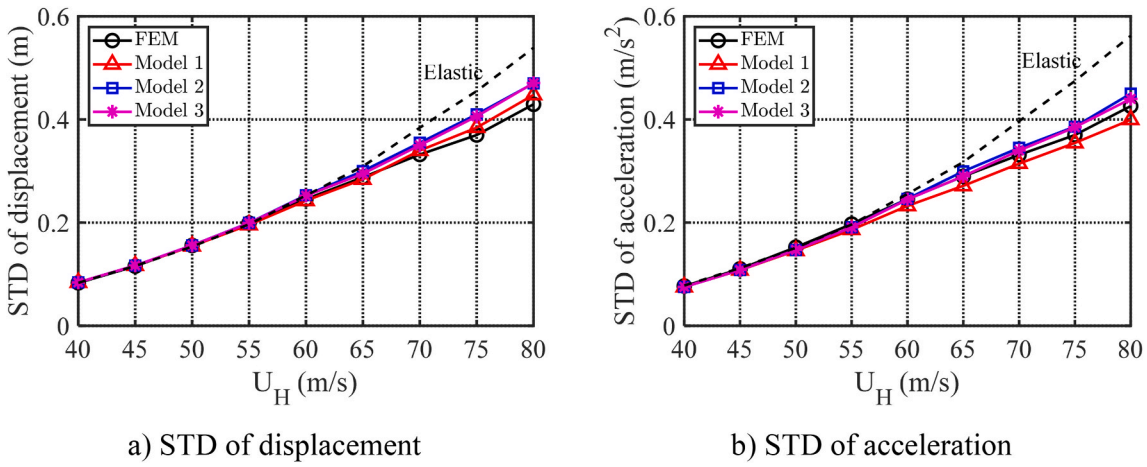

Fig. 18. STDs of alongwind response under different wind speeds (biaxial loads).

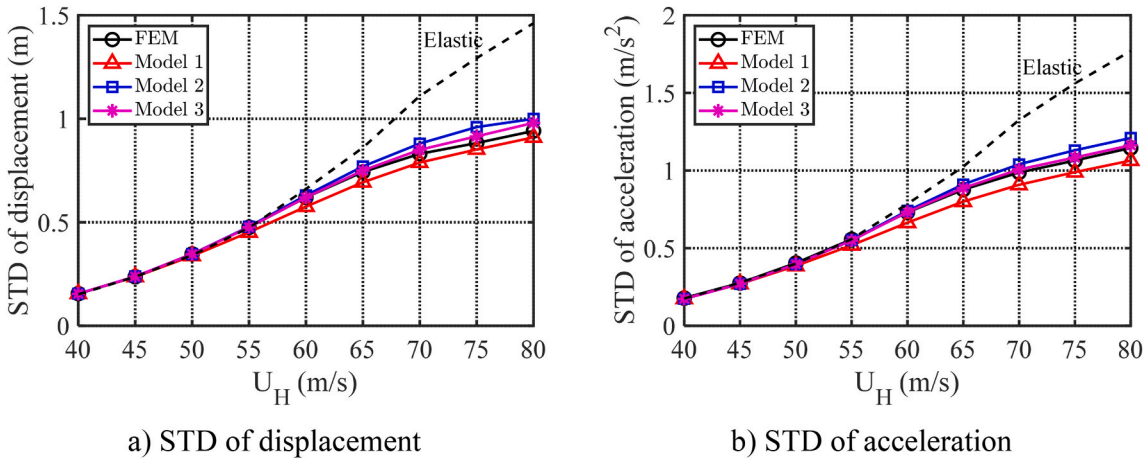

Fig. 19. STDs of crosswind response under different wind speeds (biaxial loads).

5. Characteristics of inelastic building response

5.1. Uniaxial loads

The building responses under alongwind and crosswind loads acting separately (uniaxial loads) are firstly evaluated and will be compared to the case under both loads acting simultaneously (biaxial loads). The response time history is computed using the Runge-Kutta method with a time step of 0.04 s. The building is assumed to be at rest at beginning. The 10-min mean wind speed at the building top varies from 40 to 80 m/s. Fig. 6 shows the time histories of alongwind building top displacement at $U_H = 80$ m/s calculated from different models using same loading histories. A longer time duration of response is calculated using the reduced-order models to reach the steady-state displacement. It is evident that the alongwind displacement exhibits time-varying mean component, which is sensitive to the hysteretic restoring force model. The overestimation of Model 1 is most significant. Model 3 gives best estimation. The steady-state mean alongwind displacement is determined from the equilibrium equation under static wind force with second (post-yielding) stiffness (e.g., Feng and Chen, 2018). Models 1 and 2 have the same post-yielding stiffness, thus lead to same steady-state mean alongwind displacement. Model 3 gives a lower steady-state mean alongwind displacement as the post-yielding stiffness is higher. The time-varying mean displacement develops slower at a lower wind speed with lower yielding level. The relationship of the generalized alongwind restoring force and displacement is shown in Fig. 7. There are lots of intermediate unloading and reloading paths, indicating existence of potential artificial drift and overestimation of the time-varying mean displacement due to use of Bouc-Wen hysteretic force model. More discussions concerning the nonphysical behavior of Bouc-Wen hysteresis model will be presented in the latter part of the study.

The fluctuating displacement around the time-varying mean component can be estimated without consideration of the mean alongwind load because the hysteresis loop with non-zero mean load is simply to shift the average center position of the loop from the origin to a new position without the change of the shape (e.g., Roberts and Spanos, 2003; Feng and Chen, 2018; Huang and Chen, 2023). Fig. 8 shows the comparison of alongwind building top displacement calculated from different models without consideration of the mean loads using the same alongwind loading time history. Fig. 9 portrays the STDs of alongwind building top displacement $\sigma_{q_y} = \sigma_y$ and acceleration at different wind speeds. The STD of fluctuating response at a given wind speed is computed from 50 response history samples with a duration of 900 s through ensemble average. The time history at the first 300 s is removed in analysis to avoid the transient effect. The STD of corresponding linear elastic response is also given.

Fig. 10 displays the comparison of crosswind building top displacement calculated from different models at $U_H = 80$ m/s. The crosswind displacement does not have time-varying mean component. Fig. 11 shows the relation of hysteretic crosswind restoring force and displacement. There is no intermediate unloading and reloading path. Fig. 12 displays the STDs of crosswind building top displacement $\sigma_{q_x} =$

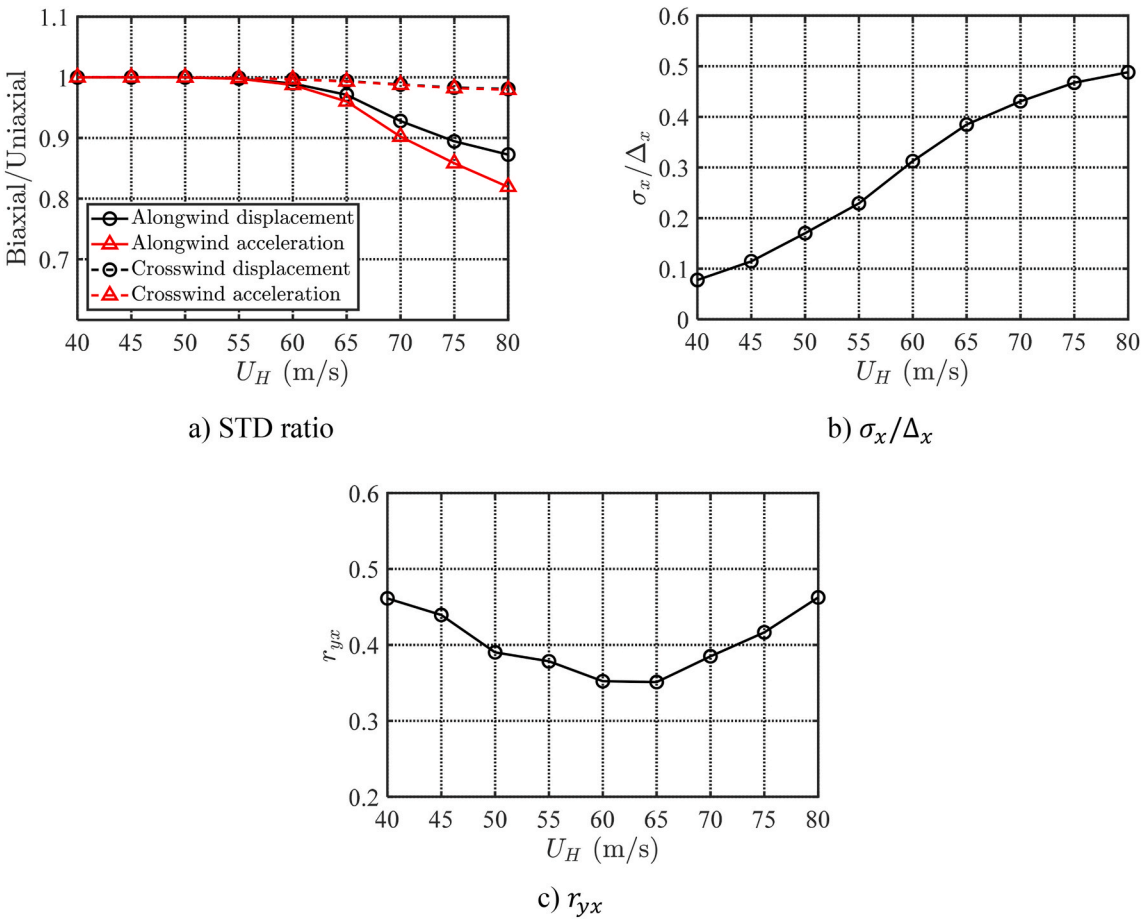

Fig. 20. Biaxal effects on building displacement and acceleration (Model 3).

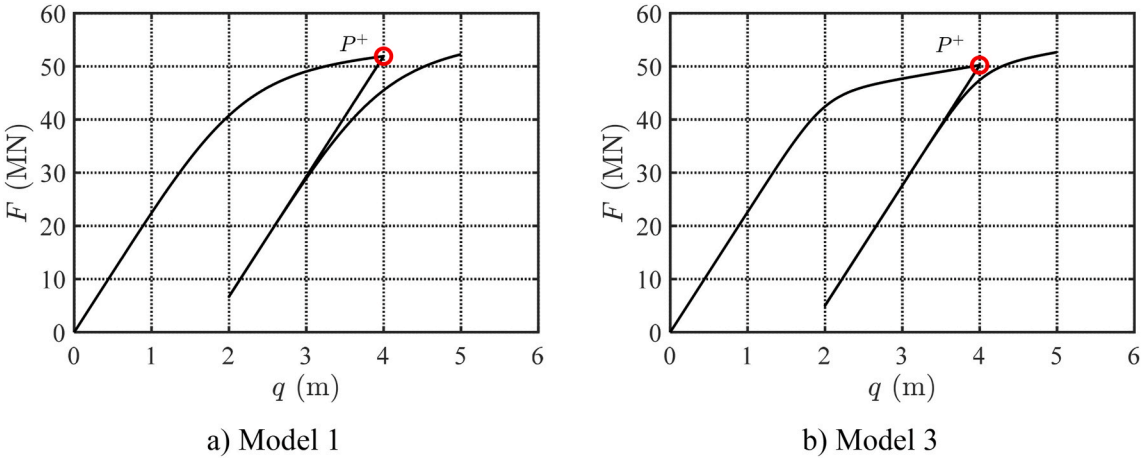

Fig. 21. Illustration of nonphysical displacement drift of Bouc-Wen model during an intermediate unloading and reloading path.

σ_x and acceleration at different wind speeds. Table 2 compares the response STDs at $U_H = 80$ m/s.

It is evident that the FE model and reduced-order models give very close estimations of response STDs. The STD of alongwind response is very close to that of elastic response. On the other hand, the inelastic crosswind response at a higher wind speed corresponds to a higher level of yielding and is lower than the corresponding elastic response attributed to the effect of additional hysteretic damping. It is confirmed that the fluctuating responses predicted from reduced-order models are not sensitive to the hysteretic model parameters as the three models provide very consistent hysteretic damping. The Model 3 gives the best estimation.

5.2. Biaxial loads

Fig. 13 shows the time histories of alongwind building top displacement at $U_H = 80$ m/s under biaxial loads, where the time-varying mean component grows faster to steady-state level than that under uniaxial loads. Again, Model 3 gives the best estimation. Model 2 is better than Model 1 but both models lead to identical steady-state

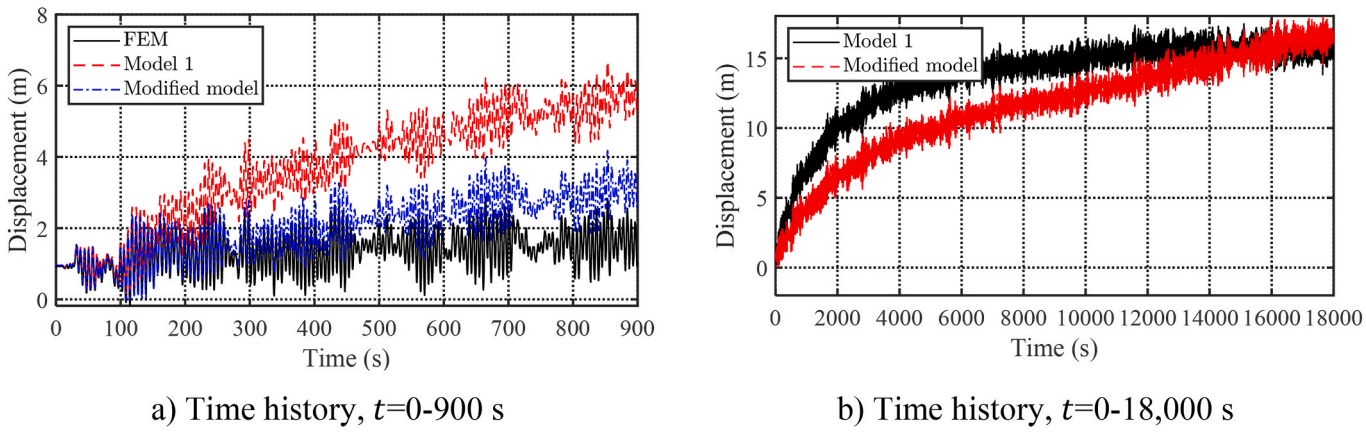

Fig. 22. Time-varying mean alongwind displacement using a modified model (uniaxial loads, $U_H = 80$ m/s).

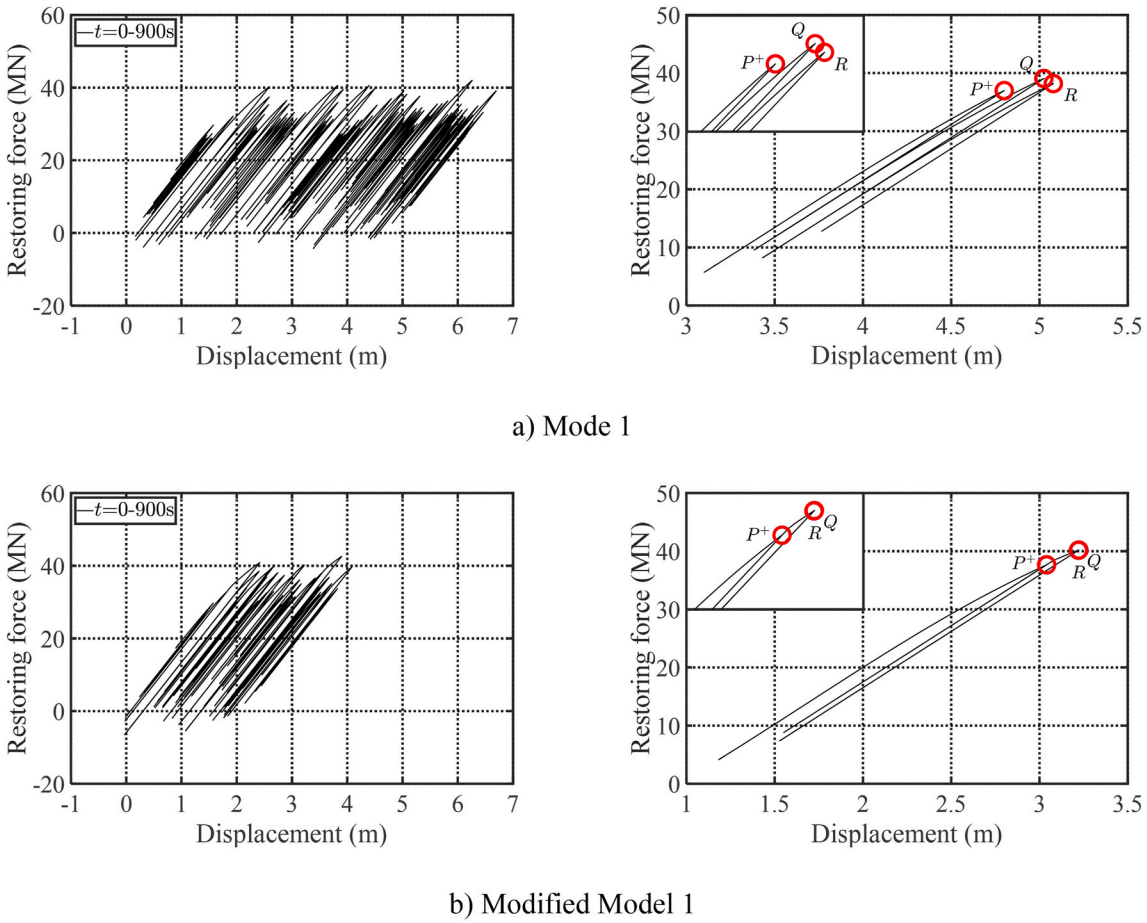

Fig. 23. Relation of alongwing hysteretic force and displacement relation using a modified model (uniaxial loads, $U_H = 80$ m/s).

alongwind displacement. The biaxial interaction does not affect the steady-state mean alongwind displacement. Fig. 14 shows the alongwind restoring force-displacement relation from three models at $U_H = 80$ m/s, which are quite different from that under uniaxial loads as the relation is affected by both alongwind and crosswind responses. Fig. 15 displays the time histories of alongwind building top displacement without the mean loads.

Fig. 16 are the time histories of crosswind building top displacement. Fig. 17 shows the crosswind restoring force-displacement relation from three reduced-order models. The fluctuating responses estimated from different models are very close to each other, but the time-varying mean alongwind displacement is sensitive to the hysteretic force models.

Figs. 18 and 19 portray the STDs of the building top displacement and acceleration. Table 2 also listed the comparison of STDs at $U_H = 80$ m/s. The biaxial interaction leads to increased level of yielding in alongwind direction, thus more reduction of alongwind displacement and acceleration. The crosswind response, which is much greater than fluctuating alongwind response, is almost not affected by biaxial interaction. The response skewness and peak factor estimated from different models are also very close.

Fig. 20 shows the ratio of response STD under biaxial loads to that under uniaxial loads estimated from Model 3. The yielding level of

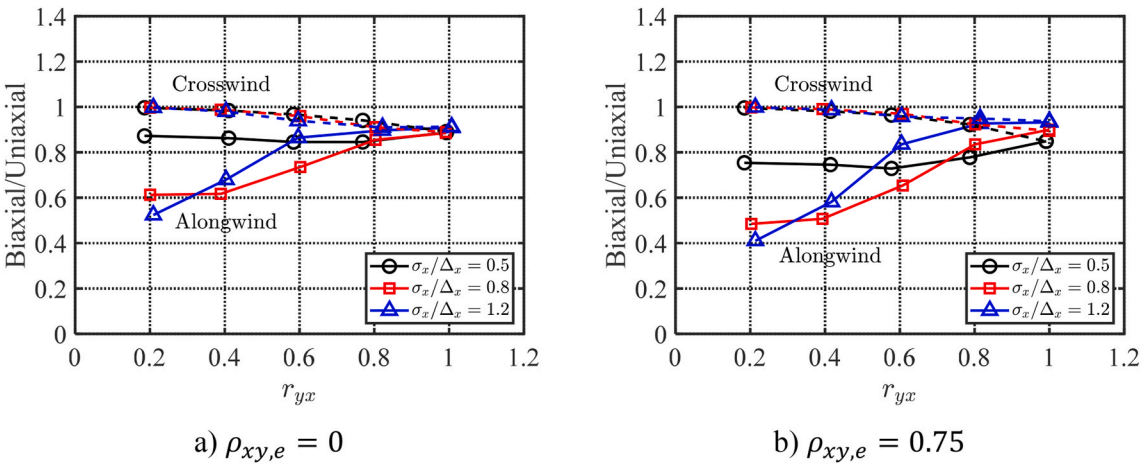

Fig. 24. Influence of biaxial interaction on alongwind and crosswind displacements.

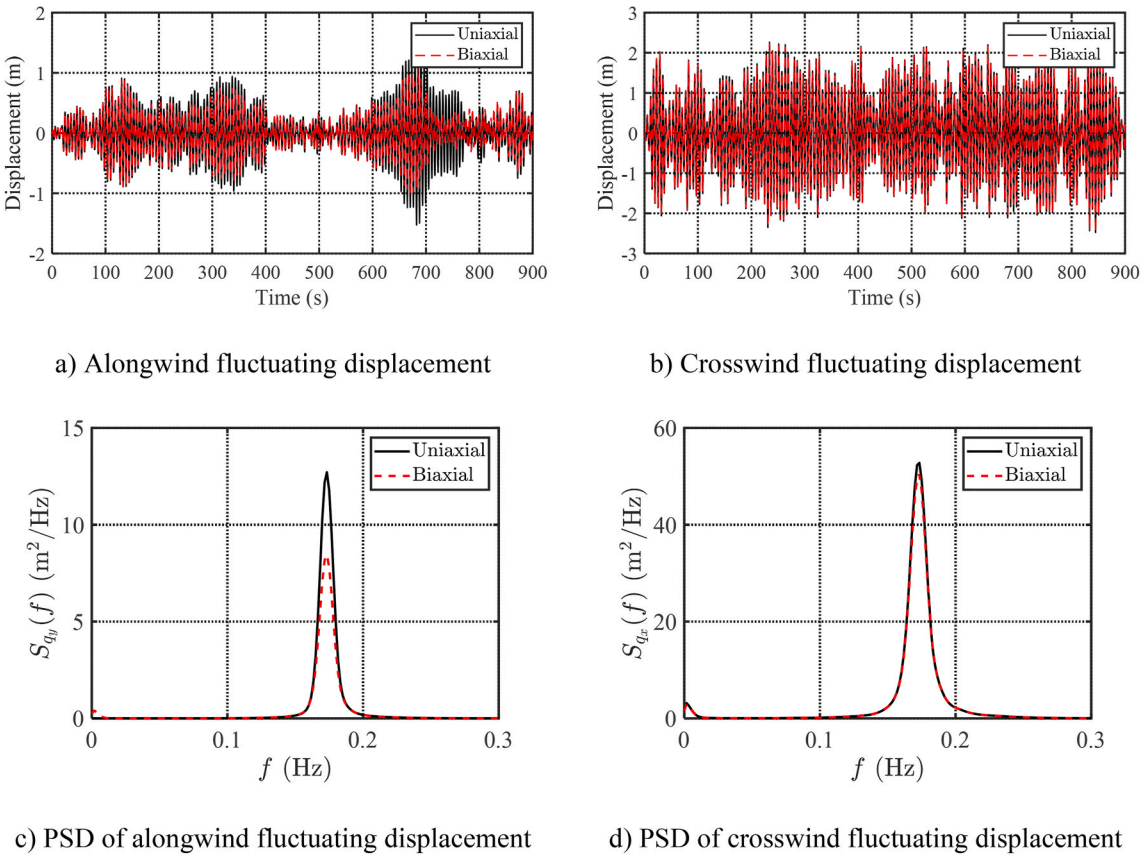

Fig. 25. Time histories and PSDs of the building top fluctuating displacements ($\sigma_x/\Delta_x = 0.5$, $r_{yx} = 0.41$, and $\rho_{xy,e} = 0$).

crosswind displacement in terms of σ_x/Δ_x and response ration $r_{yx} = (\sigma_y/\Delta_y)/(\sigma_x/\Delta_x)$ are also shown. The biaxial interaction has negligible influence on crosswind response, while it leads to a reduction in alongwind response as compared to the case under uniaxial loads. For instance, at $U_H = 80$ m/s, the normalized STDs of alongwind and crosswind displacements under uniaxial loads are $\sigma_y/\Delta_y = 0.23$ and $\sigma_x/\Delta_x = 0.51$. Under the biaxial loads, $\sigma_y/\Delta_y = 0.20$ and $\sigma_x/\Delta_x = 0.48$. The STDs of alongwind displacement and acceleration are reduced by 13% and 18%, respectively.

6. Modified uniaxial hysteretic restoring force model

The Bouc-Wen model exhibits displacement drift, force relaxation and nonclosure of hysteretic loops during an intermediate unloading and reloading path. For purpose of illustration, Fig. 21 shows the alongwind restoring force and displacement relation using Models 1 and 3 for the prescribed displacement path $q = [0 \rightarrow 1 \rightarrow 2 \rightarrow 3 \rightarrow 4 \rightarrow 3 \rightarrow 2 \rightarrow 3 \rightarrow 4 \rightarrow 5]$ m. In the following, the sub-index y of variables is ignored for simplicity. An unloading and reloading path starts at a positive reversal point P^+ with $q = 4$ m. Physically, the reloading path $q = [2 \rightarrow 3 \rightarrow 4 \rightarrow 5]$ m should follow the same path of unloading until reaching the reversal point. However, the Bouc-Wen

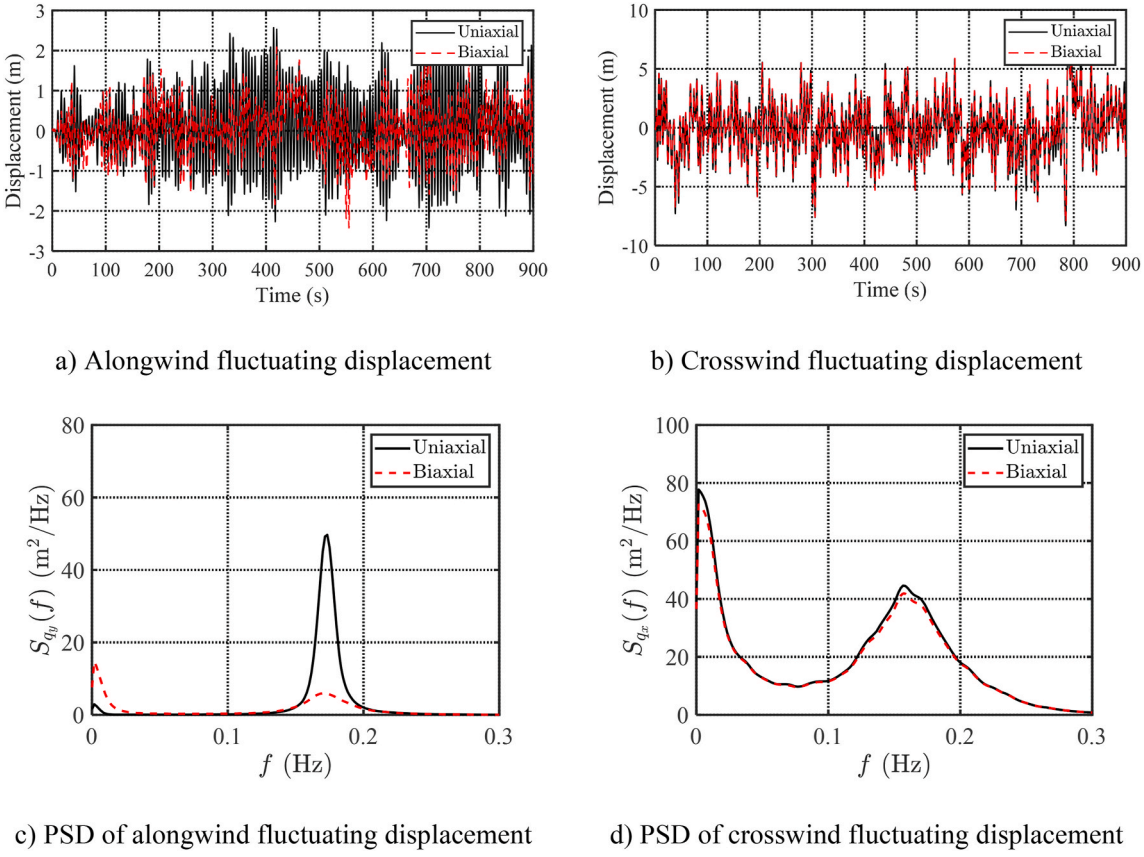

Fig. 26. Time histories and PSDs of the building top fluctuating displacements ($\sigma_x/\Delta_x = 1.2$, $r_{yx} = 0.40$, and $\rho_{xy,e} = 0$).

Table 3
Background and resonant components of alongwind and crosswind fluctuating displacements.

Yielding level		$\sigma_x/\Delta_x = 0.5$				$\sigma_x/\Delta_x = 1.2$			
Response ratio		$r_{yx} = 0.19$		$r_{yx} = 0.41$		$r_{yx} = 0.21$		$r_{yx} = 0.40$	
STD		σ_B	σ_R	σ_B	σ_R	σ_B	σ_R	σ_B	σ_R
Uniaxial	Alongwind	0.003	0.188	0.007	0.415	0.008	0.501	0.137	0.964
	Crosswind	0.148	0.997	0.147	0.999	1.322	1.998	1.351	2.002
Biaxial	Alongwind	0.020	0.163	0.048	0.354	0.161	0.209	0.387	0.542
($\rho_{xy,e} = 0$)	Crosswind	0.147	0.993	0.143	0.982	1.319	1.993	1.321	1.967
Biaxial	Alonwind	0.020	0.140	0.045	0.309	0.134	0.167	0.345	0.470
($\rho_{xy,e} =$ 0.75)	Crosswind	0.160	0.991	0.158	0.972	1.375	1.999	1.296	1.974

model does not differentiate between virgin loading and reloading, and provides a reduced stiffness of the reloading path, thus leads to a nonphysical displacement drift. Obviously, this displacement drift is larger in Model 1 than that in Model 3.

Charalampakis and Koumousis (2009) introduced a stiffening factor R_s to increase the reloading stiffness of the uniaxial hysteretic model. The uniaxial hysteretic model is revised as follows:

$$F = \alpha K q + (1-\alpha) K z \tag{10a}$$

$$\dot{z} = A\dot{q} - zI \tag{10b}$$

$$I = |\dot{q}||z|^{n-1}\{\beta_0[1 - 2H(\dot{q}z)R_s(q,z)] + \gamma_0 \mathrm{sgn}(\dot{q}z)\} \Big/ \Delta^n \tag{10c}$$

$$R_s(q,z) = H\left(z_p^+ - z\right)H(q_c - q\,)H(z)\left(\frac{q_p^+ - q_c(z)}{q_p^+ - q}\right)^p \tag{10d}$$

$$q_c(z) = \left(z - z_p^+\right) + q_p^+ (\text{for } \beta_0 = \gamma_0) \tag{10e}$$

where $R_s(q,z) \in [0,1]$ is a stiffening factor; $H(\bullet)$ is the Heaviside function defined as $H(x) = 1$ for $x > 0$ and $H(x) = 0$ for $x \le 0$; $P^+(q_p^+, z_p^+)$ is a positive reversal point in the $q - z$ space with $z > 0$ from where the unloading is started; $C(q_c, z)$ is the point of unloading path corresponding to current point $A(q_c, z)$ as in the $q - z$ space; parameter p is the parameter that controls the intensity of stiffening and realistic hysteretic behavior can be achieved for p between 1 and 2.

For the negative reversal point, $P^-(q_p^-, z_p^-)$ in the $q - z$ space with $z < 0$, $R_s(q,z)$ and $q_c(z)$ can be calculated as follows by symmetry:

$$R_s(q,z) = H\left(z - z_p^-\right)H(q - q_c\,)H(-z)\left(\frac{q_p^- - q_c(z)}{q_p^- - q}\right)^p \tag{11a}$$

$$q_{yc}(z) = \left(z - z_p^-\right) + q_p^- \tag{11b}$$

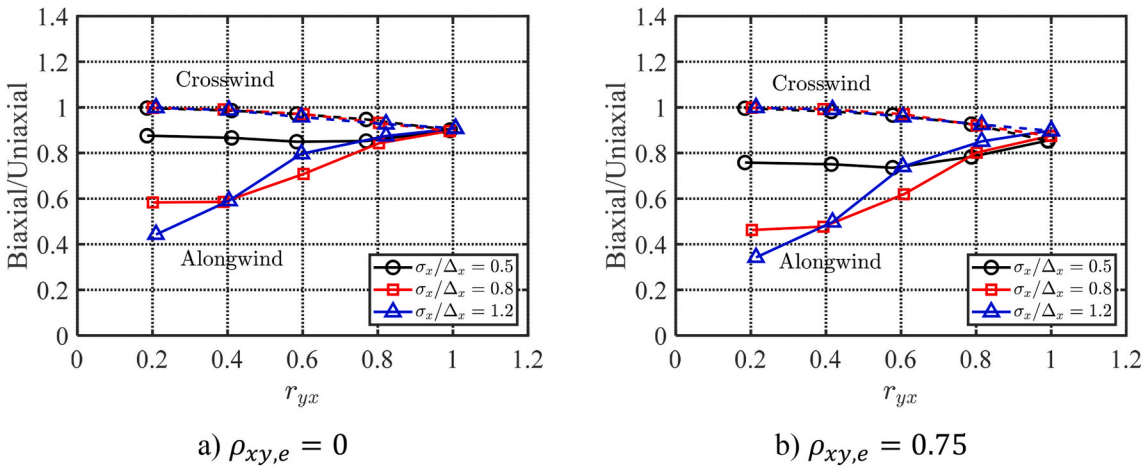

Fig. 27. Influence of biaxial interaction on alongwind and crosswind accelerations.

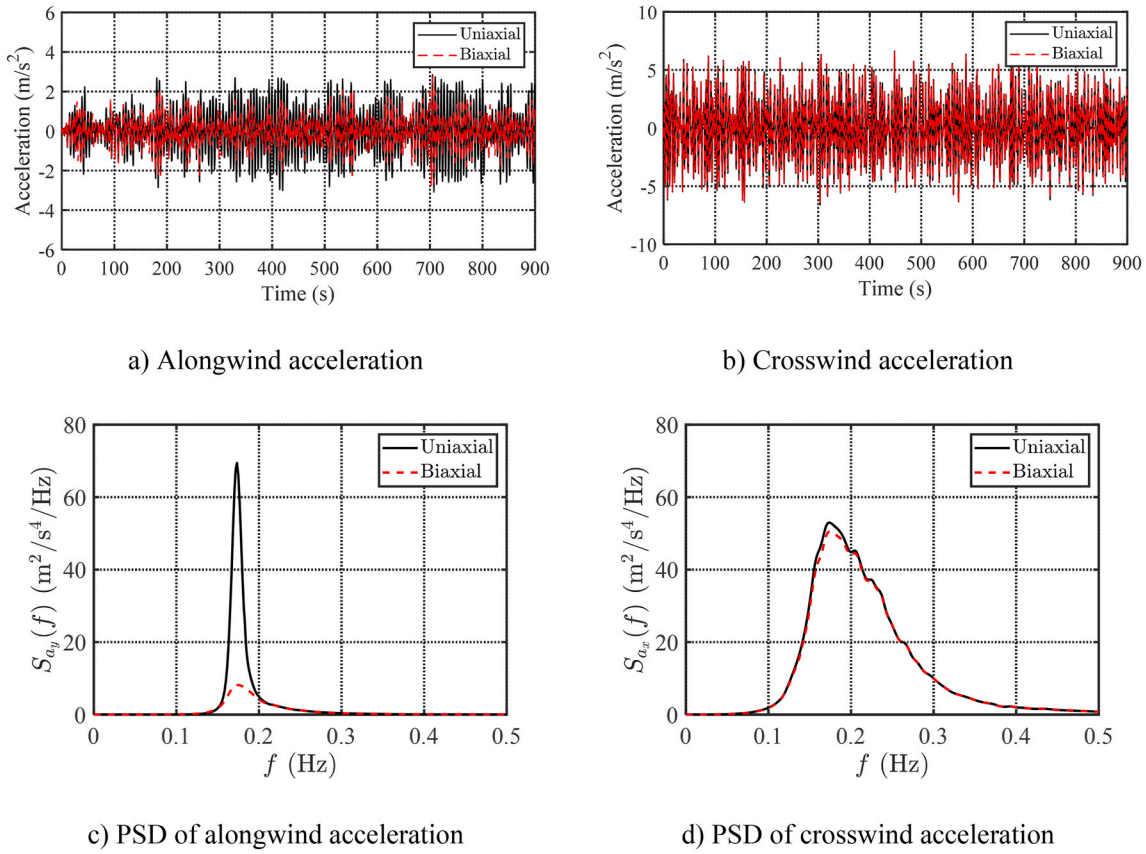

Fig. 28. Time histories and PSDs of the building top accelerations ($\sigma_x/\Delta_x = 1.2$, $r_{yx} = 0.40$, and $\rho_{xy,e} = 0$).

For the negative reversal point, $P^-(q_p^-, z_p^-)$ in the $q-z$ space with $z < 0$, $R_s(q,z)$ and $q_c(z)$ can be calculated as follows by symmetry:

$$R_s(q,z) = H\left(z - z_p^-\right) H(q - q_c) H(-z) \left(\frac{q_p^- - q_c(z)}{q_p^- - q}\right)^p \tag{12a}$$

$$q_{yc}(z) = \left(z - z_p^-\right) + q_p^- \left(\text{for } \beta_0 = \gamma_0\right. \tag{12b}$$

The modified model only changes the reloading stiffness while the unloading stiffness remains unchanged via the introduction of Heaviside function $H(\dot{q}z)$. For $R_s(q,z) = 1$, the reloading stiffness becomes equal to the unloading stiffness at the same point. For $R_s(q,z) = 0$, the modified model is the same with the original model. The reversal point $P^+(q_p^+, z_p^+)$ is defined to ensure the virgin loading stiffness is not affected. Only the reloading stiffness is increased until reaching the level of z_p^+ by the introduction of Heaviside function $H(z_p^+ - z)$.

Three methods can be used to define the reversal points for a random vibration, i.e., last observed reversal point, reversal point with maximum displacement and multiple reversal points (Charalampakis and Koumousis, 2009). The last observed reversal point corresponds to the last observed extrema with its hysteretic displacement being positive for the local maxima and negative for the local minima. If there are more than one reversal point, the one with maximum displacement can be selected as the reversal point. These two methods may not correct the

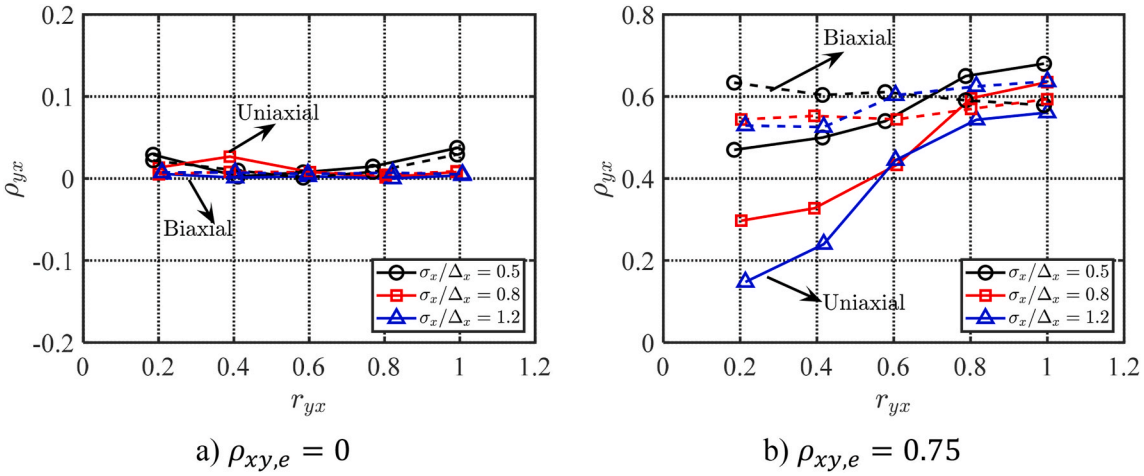

Fig. 29. Influence of biaxial interaction on correlation coefficient of alongwind and crosswind fluctuating displacements.

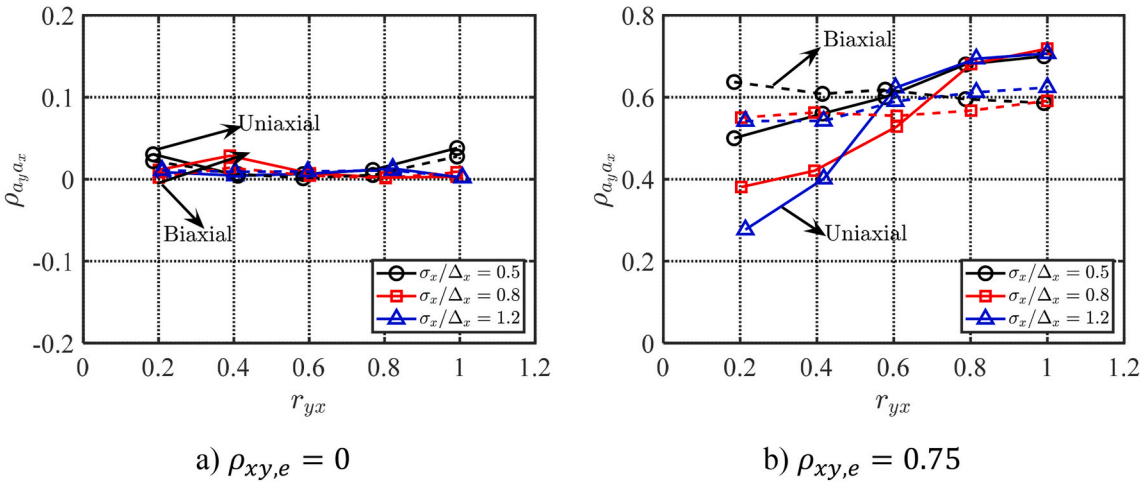

Fig. 30. Influence of biaxial interaction on correlation coefficient of alongwind and crosswind accelerations.

reloading path for all cases, so multiple reversal points should be considered. The stiffening factors for all reversal points were calculated and the reversal point corresponds with the largest R_s was selected as the "active" reversal point in the analysis. For general random vibration, a more comprehensive approach can be used to define the reversal point (Charalampakis and Koumousis, 2009). For the narrow-band alongwind response addressed in this study, the reversal point can be readily identified and multiple reversal points were used in the analysis.

Fig. 22 shows the inelastic alongwind displacement from FE model, Model 1 and modified Model 1 under uniaxial loads at $U_H = 80$ m/s. The hysteretic restoring force-displacement relation estimated from Model 1 and its modified version is shown in Fig. 23. The relation zoomed during a short time duration $t = 422$ s–440 s is also displayed, which includes two intermediate unloading and reloading paths started from the reversal point P^+ and ended at point Q, and then from point Q to point R. In the original Model 1 the reloading path cannot follow the previous unloading path thus leads to nonphysical drift. The modified model shows effectiveness to correct the nonphysical behavior and to eliminate the displacement drift. The accumulation of this elimination during larger numbers of intermediate unloading and reloading cycles is significant. The modified model greatly reduces the nonphysical drift and leads to much improved estimation of time-varying mean displacement. When the yielding level is not significant, a much longer time duration is needed for the time-varying mean displacement to reach its steady-state level. Therefore, the transient phase of time-varying men displacement is more relevant to the practical application. The improvement from the modified model is important.

It is interesting to note that the modified model does not affect the steady-state mean displacement. There is real physical displacement drift caused by virgin loading. As the time-varying mean approaches the steady-state mean, less intermediate unloading-reloading paths are observed. The restoring force and displacement relations show full hysteresis loops, so time-varying mean stops developing.

Although this modified model is very effective for the uniaxial model, its extension to biaxial hysteresis model is non-trivial. There is no straightforward approach to identify the intermediate reloading path in the biaxial force-displacement relation and to introduce modification of reloading stiffness.

Another approach to reduce the nonphysical drift is to use a Bouc-Wen model with a large parameter n, that controls the transition region of the hysteretic relation, such as the Model 3 as shown in Fig. 21b). This approach is effective for both uniaxial and biaxial Bouc-Wen models. The only issue arises when this model is combined with the statistical linearization procedure for response estimation. The accuracy of linearization approach can be sacrificed because higher statistical moments are involved and sensitive to assumed probability distribution model.

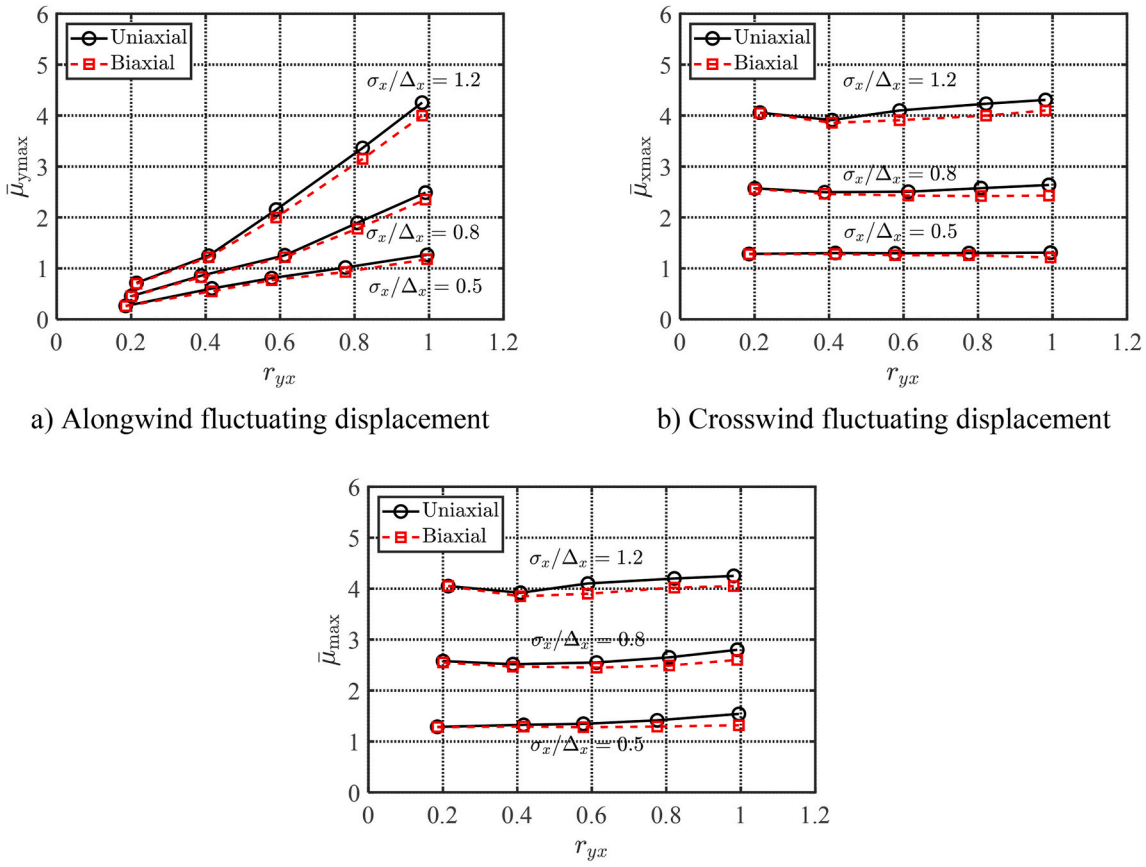

Fig. 31. Comparison of mean extremes of fluctuating displacements, $\bar{\mu}_{\text{ymax}}$, $\bar{\mu}_{\text{xmax}}$ and $\bar{\mu}_{\text{max}}$ ($\rho_{xy,e} = 0$).

7. Parametric study on biaxial interaction

7.1. Modified building and wind loading models

The biaxial effect is influenced by several parameters including yielding level in the dominant direction, i.e., crosswind direction, σ_x/Δ_x under uniaxial crosswind load; ratio of alongwind to crosswind responses under uniaxial loads, $r_{yx} = (\sigma_y/\Delta_y)/(\sigma_x/\Delta_x)$; and their correlation coefficient in terms of that of corresponding linear responses for simplicity, $\rho_{xy,e}$. When both responses are in linear elastic, there is no biaxial interaction regardless of response levels. The yielding level of the dominant crosswind response σ_x/Δ_x is an important influencing parameter. The correlation coefficient $\rho_{xy,e}$ is determined by the modal frequency ratio, damping ratios and correlation/coherence of the generalized forces (Chen and Kareem, 2005b). The correlation of alongwind and crosswind responses is weaker than the that of corresponding wind loadings. Both responses can be mutually independent when both modal frequencies are well separated even both loadings are strongly correlated.

To facilitate a comprehensive parametric study covering wider ranges of influencing parameters, a modified building model is adopted. It is assumed that the building has same dynamic characteristics in two translational directions which take the values of the 60-story building in crosswind (x-) direction, i.e., $f_x = f_y = 0.173$ Hz, $\zeta_x = \zeta_y = 1\%$, $M_x = M_y$, $K_x = K_y$, and $B = D = 30.48$ m. The biaxial hysteresis model parameters are $\Delta_x = \Delta_y = 2.0$ m, $\alpha_x = \alpha_y = 0.11$ and $n = 9$. This refined building model is expected to have greater biaxial interaction than the original building model. To examine the influence of correlation of responses, the generalized alongwind and crosswind loads $Q_y(t)$ and $Q_x(t)$ are assumed to have same PSD shapes and with a correlation coefficient of $\rho_{Q_{xy}}$. They are given as $Q_x(t) = \Gamma_x Q_1(t)$ and $Q_y(t) = \Gamma_y Q_1(t)\rho_{Q_{xy}} + \Gamma_y Q_2(t)\sqrt{1-\rho^2_{Q_{xy}}}$, where $Q_1(t)$ and $Q_2(t)$ are independent and have same PSD; Γ_x and Γ_y are scaling parameters which are used to adjust the levels of alongwind and crosswind responses. In this parametric study, $\rho_{xy,e} = \rho_{Q_{xy}}$ as the building has the same dynamic modal properties in two directions. In the following analysis, the crosswind loading spectrum of square-shaped building at $U_H = 80$ m/s is used for generating time histories of $Q_1(t)$ and $Q_2(t)$. For each case study, 50 response history samples with time duration of 900 s under zero mean alongwind load are simulated for estimating the response statistics through the reduced-order building model and the first 300 s is removed to avoid the transient effect.

Use of this modified building model facilitates adjusting values of the controlling parameters. In the case of the original building, the parameters have very limited ranges for the investigated range of mean wind speeds and direction as shown in Fig. 20b) and c). The results gained from this parametric study with nondimensional parameters shed insights which can equally be applied to various buildings and wind directions.

7.2. Response STDs

Fig. 24 displays the ratio of response STD under biaxial loads to that under uniaxial loads for alongwind (y-direction) and crosswind (x-direction) fluctuating displacements as a function of σ_x/Δ_x, r_{yx}, and $\rho_{xy,e}$, where the solid lines and dashed lines represent the results of alongwind and crosswind responses, respectively. In this parametric study, the crosswind response is larger than the alongwind response. It is observed

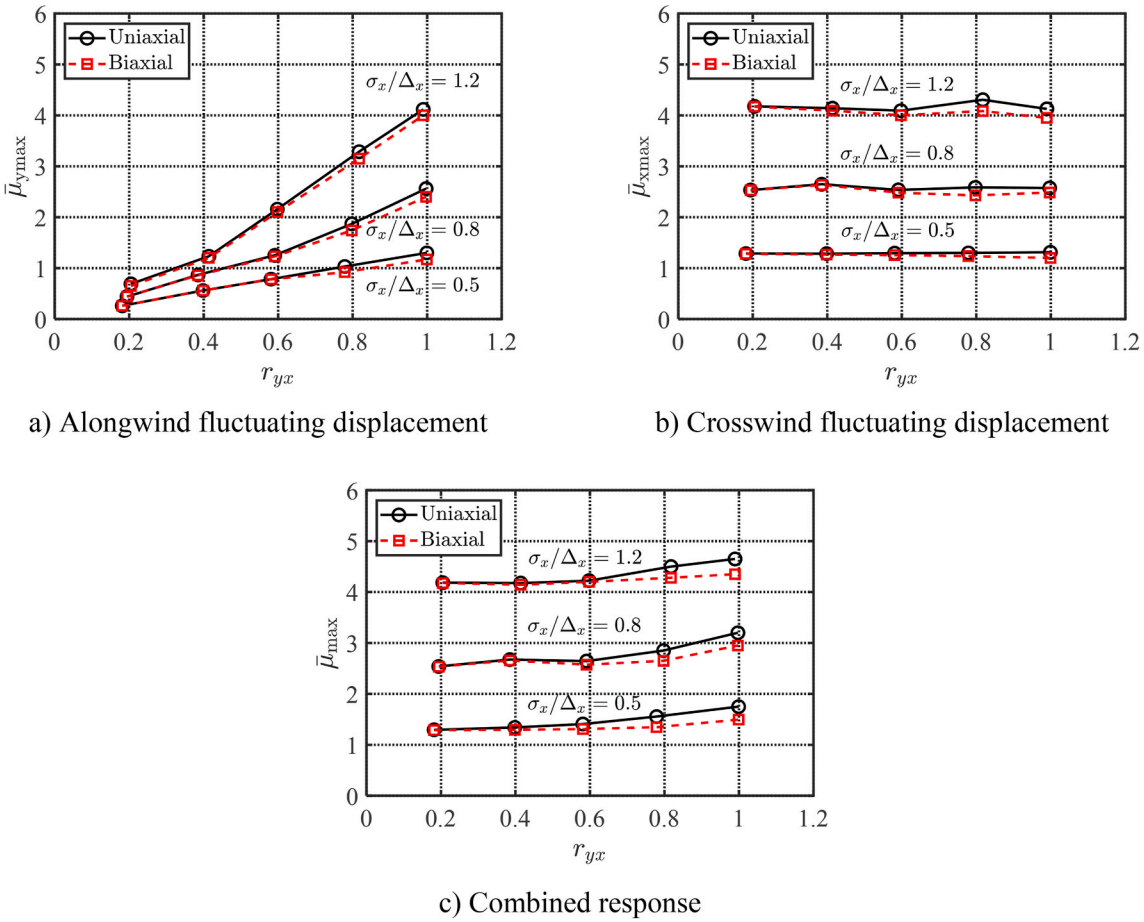

Fig. 32. Comparison of mean extremes of fluctuating displacements, $\bar{\mu}_{ymax}$, $\bar{\mu}_{xmax}$ and $\bar{\mu}_{max}$ ($\rho_{xy,e} = 0.75$).

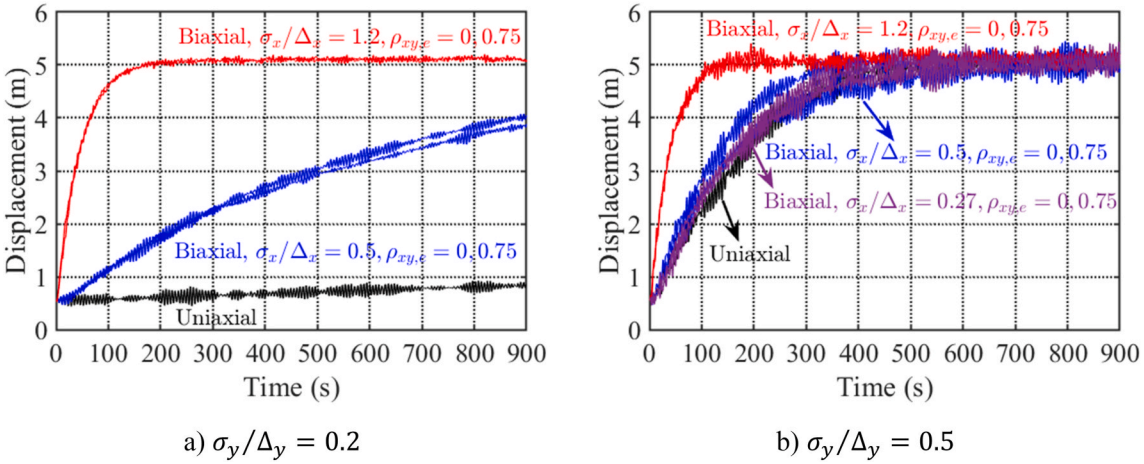

Fig. 33. Influence of response ratio on time-varying mean displacement.

that the alongwind response is reduced by the biaxial effect, which is more noticeable when alongwind response is much lower than the crosswind response, i.e., a lower value of r_{yx}. The crosswind response is not affected by biaxial effect when both responses are quite different. The biaxial effect reduces when both responses are close to each other, i.e., when r_{yx} is close to unity, where both responses are slightly decreased. The biaxial effect does not monotonically increase with the increasing yielding level σ_x/Δ_x. For example, at $r_{yx} = 0.2$ and $\rho_{xy,e} = 0$, the reduction of alongwind displacement STD is 13%, 39% and 48%, respectively, for $\sigma_x/\Delta_x = 0.5$, 0.8 and 1.2. On the other hand, at $r_{yx} = 0.4$, the reduction of displacement STD is 14%, 38% and 14%. The biaxial effect slightly increases when both responses are more correlated. As discussed previously, in the case of the original building at $U_H = 80$ m/s, we have $\sigma_x/\Delta_x = 0.51$, $r_{yx} = 0.45$ and $\rho_{xy,e} = 0$. The reduction of alongwind displacement STD by biaxial interaction is 13%, which is consistent with the results presented in Fig. 24a).

Fig. 25 shows the time histories of fluctuating displacements and power spectra at $\sigma_x/\Delta_x = 0.5$ and $r_{yx} = 0.41$. Fig. 26 is results at $\sigma_x/$

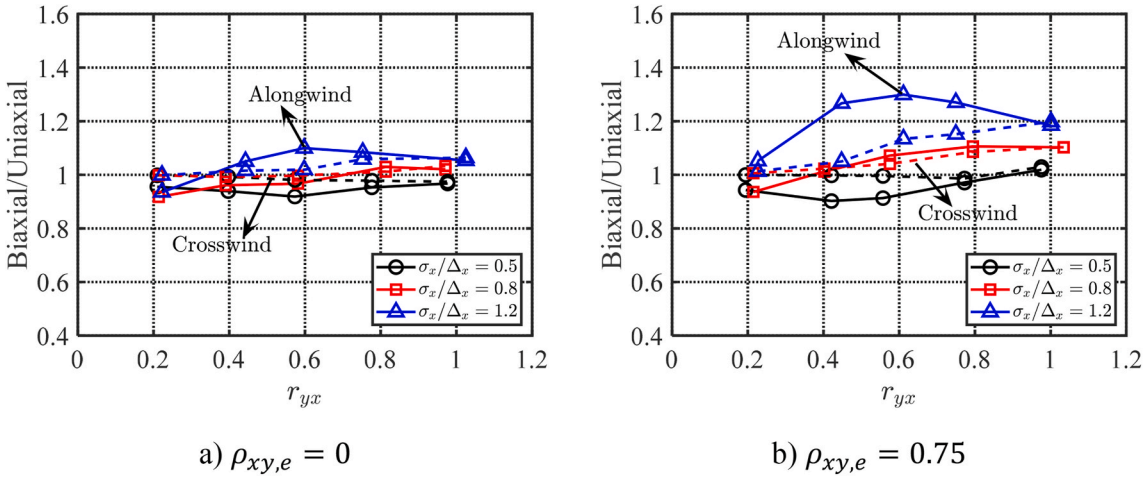

Fig. 34. Influence of biaxial interaction on alongwind and crosswind fluctuating displacements (use of alongwind loading spectrum).

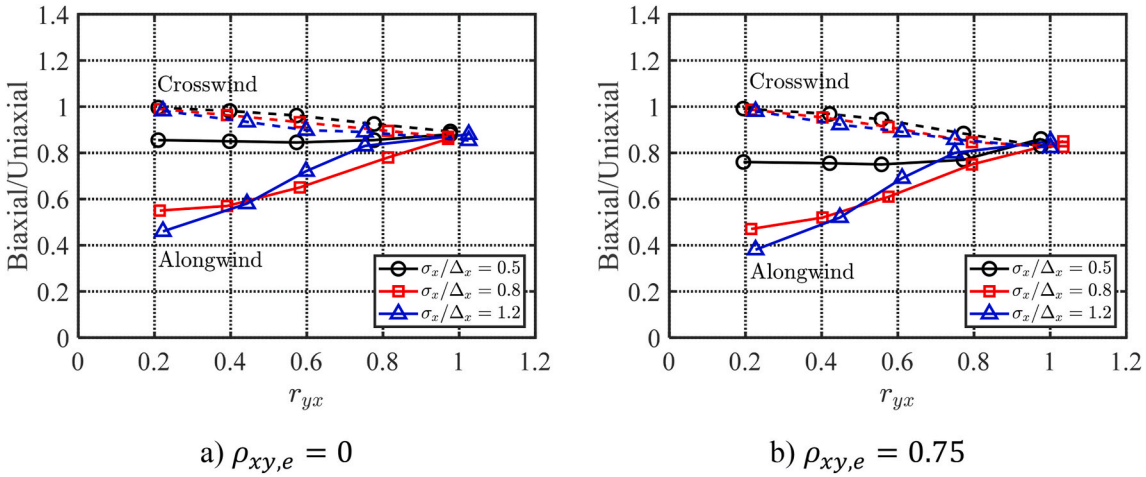

Fig. 35. Influence of biaxial interaction on alongwind and crosswind accelerations (use of alongwind loading spectrum).

$\Delta_x = 1.2$ and $r_{yx} = 0.40$ with $\rho_{xy,e} = 0$. It is observed that as the yielding level increases, the resonant component of crosswind fluctuating displacement decreases due to additional hysteretic damping, while the low-frequency component of crosswind fluctuating displacement increases that is associated with the vibration corresponding to the lower post-yielding stiffness. The biaxial effect on alongwind fluctuating displacement includes two contributions, i.e., decrease in resonant component and increase in low-frequency component. Fig. 26a) and b) clearly show the coupled low-frequency component in both alongwind and crosswind fluctuating displacements.

Table 3 summarizes the STDs of low-frequency (background) and resonant fluctuating displacements under uniaxial and biaxial loads, i.e., σ_B and σ_R, where the total STD is $\sigma = \sqrt{\sigma_B^2 + \sigma_R^2}$. At $\sigma_x/\Delta_x = 0.5$, $r_{yx} = 0.41$ and $\rho_{xy,e} = 0$, the resonant alongwind fluctuating displacement σ_R is reduced by 15% due to biaxial interaction, but the ratio σ_B/σ_R is increased from 2% to 14%. At $\sigma_x/\Delta_x = 1.2$, $r_{yx} = 0.40$ and $\rho_{xy,e} = 0$, the resonant alongwind component σ_R is reduced by 44%, while σ_B/σ_R is increased from 14% to 71%. The biaxial effect only slightly increases with increasing response correlation. For instance, at $\sigma_x/\Delta_x = 1.2$, $r_{yx} = 0.40$ and $\rho_{xy,e} = 0.75$, the resonant alongwind component σ_R is decreased by 51% and σ_B/σ_R is increased from 14% to 73%.

Fig. 27 shows the influence of biaxial interaction on building accelerations. Fig. 28 displays the acceleration time histories and PSDs at $\sigma_x/\Delta_x = 1.2$, $r_{yx} = 0.40$ and $\rho_{xy,e} = 0$. As expected, the accelerations do not have low-frequency component. The biaxial interaction leads to more reduction of alongwind acceleration as compared to fluctuating displacement. The influence of biaxial interaction slightly increases when responses are more correlated.

7.3. Correlation coefficient of responses

The correlation coefficient of alongwind and crosswind responses is important for the evaluation of combined responses. Fig. 29 shows the correlation coefficient of alongwind and crosswind fluctuating displacements influenced by σ_x/Δ_x, r_{xy} and $\rho_{xy,e}$. The solid lines and dashed lines represent the results under uniaxial and biaxial loads, respectively. Fig. 30 displays the correlation coefficient of alongwind and crosswind accelerations. It is evident that the correlation coefficient of fluctuating displacements under uniaxial loads is lower than that of elastic responses. When the yielding levels of two responses are very distinct, i.e., r_{yx} is low, the corresponding structural systems in both directions under uniaxial loads become very distinct thus the correlation reduces. The correlation coefficient under biaxial loads is higher than that under uniaxial loads and becomes less sensitive to r_{yx} and σ_x/Δ_x, while is slightly lower than that of elastic responses. The correlation of acceleration responses has similar character, while the accelerations under uniaxial loads have stronger correlation than the fluctuating displacements.

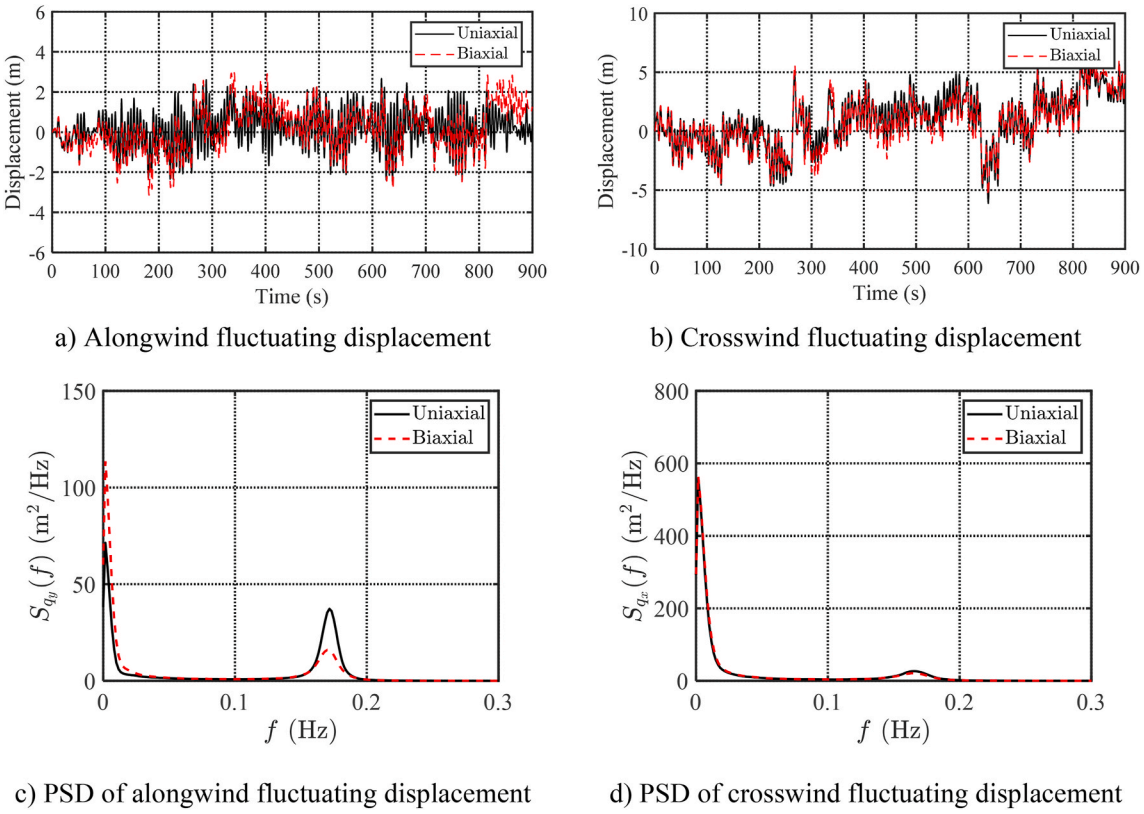

Fig. 36. Time histories and PSDs of the building top fluctuating displacements ($\sigma_x/\Delta_x = 1.2$, $r_{yx} = 0.42$, and $\rho_{xy,e} = 0.75$; use of alongwind loading spectrum).

7.4. Response extremes

The means of peak ductility demands from 50 response samples with duration of 600 s for crosswind and alongwind responses and their combined response, $\mu_{\text{xmax}} = \max_{\text{For all t}} \mu_x(t)$, $\mu_{\text{ymax}} = \max_{\text{For all t}} \mu_y(t)$, and $\mu_{\text{max}} = \max_{\text{For all t}} \mu(t)$, i.e., $\overline{\mu}_{\text{xmax}}$, $\overline{\mu}_{\text{ymax}}$ and $\overline{\mu}_{\text{max}}$, are also computed as shown in Figs. 31 and 32, and the influence of biaxial interaction is examined. The biaxial interaction leads to increase in peak factor of alongwind fluctuating displacement when r_{yx} is low. As a result, the biaxial interaction has less influence on the mean peak ductility demand as compared to the STD of alongwind fluctuating displacement. The peak ductility demand of combined response is dominated by crosswind response thus is almost not affected by biaxial interaction. Similar characters are observed for accelerations.

7.5. Alongwind time-varying mean displacement

The biaxial interaction on the time-varying mean alongwind displacement is also investigated. The time-varying mean alongwind displacement is calculated from the difference of responses with and without the mean (static) alongwind load. 50 samples are simulated to obtain their ensemble average. It should be noted that the same static alongwind load at $U_H = 80$ m/s is used in this parameter study. Fig. 33 shows the time-varying mean alongwind displacement with $\sigma_y/\Delta_y = 0.2$ and 0.5 under uniaxial loads and biaxial loads. The development rate of time-varying mean alongwind displacement to its steady-state value increases with increasing σ_y/Δ_y. At $\sigma_y/\Delta_y = 0.2$, the yielding in alongwind direction under alongwind load only is very low, thus much longer time duration is required to reach steady-state mean. On the other hand, at $\sigma_y/\Delta_y = 0.5$, the higher level of yielding leads to faster development of time-varying mean to its steady-state level.

The biaxial interaction leads to faster growth of time-varying mean alongwind displacement when the crosswind response is greater than alongwind response, i.e., $\sigma_x/\Delta_x > \sigma_y/\Delta_y$. The biaxial effect is more significant when crosswind yielding level σ_x/Δ_x is higher and the alongwind yielding level σ_y/Δ_y is lower. The response correlation has less effect on the time-varying mean. The steady-state alongwind displacement is not affected by biaxial interaction. When crosswind response is lower than alongwind response, the biaxial effect on both fluctuating and time-varying mean component of alongwind displacement is not noticeable.

7.6. Influence of loading spectrum

As discussed previously, the biaxial interaction on response is related to the background and resonant components of response, which are not only affected by level of yielding but also by the loading spectra. In the following, similar analysis is also carried out using the alongwind loading spectrum in Fig. 4 for modeling both alongwind and crosswind loadings but with different magnitudes in both directions.

Figs. 34 and 35 display the STD ratio of responses under biaxial loads to that under uniaxial loads. The influence of biaxial interaction on acceleration response is not affected by the shape of loading spectra. The alongwind fluctuating displacement is only slightly reduced by the biaxial interaction and even increased when the yielding level of crosswind response is high, especially when both alongwind and crosswind responses have strong correlation. Fig. 36 shows the response time histories and PSDs for the case with $\sigma_x/\Delta_x = 1.2$, $r_{yx} = 0.42$, and $\rho_{xy,e} = 0.75$. As compared to Fig. 26, the crosswind fluctuating displacement has more low-frequency background component. As a result, the biaxial interaction leads to more increase in low-frequency component of alongwind fluctuating displacement, which is greater than the decrease in the resonant component. Accordingly, the alongwind fluctuating displacement is increased. On the other hand, the alongwind acceleration, which has only the resonant component, is reduced due to biaxial interaction.

8. Conclusions

The time-varying mean of inelastic alongwind displacement is sensitive, but both fluctuating alongwind and crosswind inelastic responses are insensitive to the hysteretic restoring force model used in the 2DOFs reduced-order model developed by modal push-over analysis. The accumulation of nonphysical drift of Bouc-Wen hysteretic model during intermediate unloading and reloading cycles is responsible for the overestimation of time-varying mean alongwind displacement. A modified uniaxial Bouc-Wen model can effectively eliminate the nonphysical drift, but its extension to a biaxial hysteretic model is non-trivial. Use of a hysteretic model with a sharp transition from elastic to plastic regions can greatly reduce the nonphysical drift for both uniaxial and biaxial models. With this improved modeling, the reduced-order model is very accurate and computational effective for inelastic response analysis as compared to the nonlinear FE building model with distributed plasticity that is computationally very expensive.

The hysteretic restoring forces in two translational directions are affected by both responses in both directions thus the equations of motion are coupled with biaxial interaction. The crosswind response, which is larger than the fluctuating alongwind response, is only slightly reduced when both alongwind and crosswind fluctuating responses are close to each other. The biaxial interaction leads to faster growth of the time-varying mean alongwind displacement. When crosswind fluctuating displacement is lower than alongwind fluctuating displacement, the biaxial effect on time-varying mean alongwind displacement is not noticeable. The steady-state mean alongwind displacement is determined by the mean wind load and post-yielding stiffness and is not affected by biaxial interaction.

The biaxial interaction results in an increase in the low-frequency component but decrease in the resonant component of alongwind fluctuating displacement. The biaxial effect is more significant when yielding level of crosswind response is high and both responses are more distinct. The biaxial effect leads to more reduction in alongwind acceleration than alongwind fluctuating displacement. The correlation of alongwind and crosswind fluctuating displacements only slightly affects the biaxial interaction. The biaxial effect results in more correlation between alongwind and crosswind responses. The biaxial interaction effect on the alongwind displacement is also affected by loading and response spectra. The increase in the low-frequency fluctuating alongwind displacement is increased when the dominant crosswind response has more low-frequency contributions. The peak ductility demand contributed by both alongwind and crosswind responses is dominated by the larger crosswind response thus is almost not affected by the biaxial interaction.

The new insights of this study developed from a 60-story steel building example and the modified building model can also be helpful for understanding the inelastic performance of other wind-excited tall buildings under different wind directions as the inelastic responses are governed by the same equations and their characteristics can be described using non-dimensional quantities.

CRediT authorship contribution statement

Jinghui Huang: Methodology, Formal analysis, Data curation, Software, Writing – original draft. **Xinzhong Chen:** Supervision, Methodology, Writing – review & editing.

Declaration of competing interest

The authors declare that they have no known competing financial interests or personal relationships that could have appeared to influence the work reported in this paper.

Data availability

Data will be made available on request.

Acknowledgements

The support for this work provided in part by National Science Foundation (NSF) grant No. CMMI-2153189 is greatly acknowledged.

References

Architectural Institute of Japan (AIJ), 2004. AIJ Recommendations for Load on Buildings. AIJ, Tokyo.
ASCE/SEI, 2019. Prestandard for Performance-Based Wind Design. Reston, VA.
Beck, A.T., Kougioumtzoglou, I.A., dos Santos, K.R., 2014. Optimal performance-based design of non-linear stochastic dynamical RC structures subject to stationary wind excitation. Eng. Struct. 78, 145–153.
Charalampakis, A.E., Koumousis, V.K., 2009. A Bouc-Wen model compatible with plasticity postulates. J. Sound Vib. 322 (4–5), 954–968.
Chen, X., 2013. Estimation of stochastic crosswind response of wind-excited tall buildings with nonlinear aerodynamic damping. Eng. Struct. 56, 766–778.
Chen, X., 2014a. Extreme value distribution and peak factor of crosswind response of flexible structures with nonlinear aeroelastic effect. J. Struct. Eng. 140 (12), 04014091.
Chen, X., 2014b. Analysis of crosswind fatigue of wind-excited structures with nonlinear aerodynamic damping. Eng. Struct. 74, 145–156.
Chen, X., Kareem, A., 2005a. Proper orthogonal decomposition-based modeling, analysis, and simulation of dynamic wind load effects on structures. J. Eng. Mech. 131 (4), 325–339.
Chen, X., Kareem, A., 2005b. Coupled dynamic analysis and equivalent static wind loads on buildings with three-dimensional modes. J. Struct. Eng. 131 (7), 1071–1082.
Ding, J., Chen, X., 2015. Fatigue damage evaluation of broad-band Gaussian and non-Gaussian wind load effects by a spectral method. Probabilist. Eng. Mech. 41, 139–154.
Feng, C., Chen, X., 2017. Crosswind responses of tall buildings with nonlinear aerodynamic damping and hysteretic restoring force character. J. Wind Eng. Ind. Aerod. 167, 62–74.
Feng, C., Chen, X., 2018. Inelastic responses of wind-excited tall buildings: improved estimation and understanding by statistical linearization approaches. Eng. Struct. 159, 141–154.
Gani, F., Légeron, F., 2012. Relationship between specified ductility and strength demand reduction for single degree-of-freedom systems under extreme wind events. J. Wind Eng. Ind. Aerod. 109, 31–45.
Ghaffary, A., Moustafa, M.A., 2021. Performance-based assessment and structural response of 20-story sac building under wind hazards through collapse. J. Struct. Eng. 147 (3), 04020346.
Griffis, L., Patel, V., Muthukumar, S., Baldava, S., 2013. A framework for performance-based wind engineering. In: Proc., Advances in Hurricane Engineering, pp. 1205–1216. Miami, Florida, USA.
Hart, G.C., Jain, A., 2011. Nonlinear response of tall buildings subjected to wind loads. Struct. Des. Tall Special Build. 20 (S1), 63–65.
Hong, H.P., 2004. Accumulation of wind induced damage on bilinear SDOF systems. Wind Struct. 7 (3), 145–158.
Huang, J.H., Chen, X., 2022. Inelastic performance of high-rise buildings to simultaneous actions of alongwind and crosswind loads. J. Struct. Eng. 148 (2), 04021258.
Huang, J.H., Chen, X., 2023. Inelastic response of high-rise buildings under strong winds: accuracy of reduced-order building model and influence of biaxial response interaction. J. Struct. Eng. 149 (1), 04022211.
Judd, J.P., Charney, F.A., 2015. Inelastic behavior and collapse risk for buildings subjected to wind loads. In: Structures Congress, pp. 2483–2496.
Judd, J.P., Charney, F.A., 2016. Wind performance assessment of buildings. In: Proc., Geotechnical and Structural Engineering Congress. Reston, VA.
Judd, J.P., 2018. Windstorm resilience of a 10-story steel frame office building. ASCE-ASME J. Risk Uncertainty Eng. Syst., Part A: Civ. Eng. 4 (3), 04018020.
Lee, C.S., Hong, H.P., 2010. Statistics of inelastic responses of hysteretic systems under bidirectional seismic excitations. Eng. Struct. 32 (8), 2074–2086.
McKenna, F., Scott, M.H., Fenves, G.L., 2010. Nonlinear finite-element analysis software architecture using object composition. J. Comput. Civ. Eng. 24 (1), 95–107.
Mohammadi, A., Azizinamini, A., Griffis, L., Irwin, P., 2019. Performance assessment of an existing 47-story high-rise building under extreme wind loads. J. Struct. Eng. 145 (1), 04018232.
Mooneghi, M.A., Irwin, P., Chowdhury, A.G., 2015. In: Exploratory Studies on a Bilinear Aeroelastic Model for Tall Buildings. Proc., 14th Int. Conf. Wind Eng., Porto Alegre. Brazil.
NIST, 2010. Nonlinear Structural Analysis for Seismic Design: A Guide for Practicing Engineers. NIST GCR 10-917-5. Gaithersburg, MD.
Ohkuma, T., Kurita, T., Ninomiya, M., 1997. Response estimation based on energy balance for elasto-plastic vibration of tall building in across-wind direction. In: Proc., 7th International Conference on Structural Safety and Reliability, pp. 1379–1386. Kyoto, Japan.
Ouyang, Z., Spence, S.M., 2021. Performance-based wind-induced structural and envelope damage assessment of engineered buildings through nonlinear dynamic analysis. J. Wind Eng. Ind. Aerod. 208, 104452.

Park, S., Yeo, D., 2018. Second-order effect on wind-induced structural behavior of high-rise steel buildings. J. Struct. Eng. 144 (2), 04017209.
Roberts, J.B., Spanos, P.D., 2003. Random Vibration and Statistical Linearization. Courier Corporation.
Shinozuka, M., Jan, C.M., 1972. Digital simulation of random processes and its applications. J. Sound Vib. 25 (1), 111–128.
Tamura, Y., Yasui, H., Marukawa, H., 2001. Non-elastic responses of tall steel buildings subjected to across-wind forces. Wind Struct. 4 (2), 147–162.
Thyagarajan, R.S., 1989. Modeling and Analysis of Hysteretic Structural Behavior. Ph.D. thesis. California Institute of Technology, California.
Tsujita, O., Hayabe, Y., Ohkuma, T., 1997. A study on wind-induced response for inelastic structure. In: Proc., ICOSSAR, pp. 1359–1366.
Wang, C.H., Wen, Y.K., 2000. Evaluation of pre-Northridge low-rise steel buildings. I: Modeling. J. Struct. Eng. 126 (10), 1160–1168.
Wong, C.W., Ni, Y.Q., Ko, J.M., 1994. Steady-state oscillation of hysteretic differential model. II: performance analysis. J. Eng. Mech. 120 (11), 2299–2325.